Document downloaded from:

http://hdl.handle.net/10251/66243

This paper must be cited as:

Velasco Carrau, J.; García-Nieto Rodríguez, S.; Salcedo Romero De Ávila, JV. (2015). Multi-Objective Optimization for Wind Estimation and Aircraft Model Identification. Journal of Guidance, Control, and Dynamics. 39(2):372-389. doi:10.2514/1.G001294.

The final publication is available at

http://dx.doi.org/10.2514/1.G001294

Copyright American Institute of Aeronautics and Astronautics

Additional Information

Multi-Objective Optimization for Wind Estimation and Aircraft Model Identification

J. Velasco-Carrau[1], S. García-Nieto[2], and J. V. Salcedo [3]
Instituto de Automática e Informática Industrial,

Universitat Politècnica de València, Camino de Vera s/n, 46022 Valencia, Spain

R. H. Bishop[4]
College of Engineering, University of South Florida,

4202 East Fowler Avenue ENB118 Tampa, FL 33620-5350, USA

In this paper, a novel method for aerodynamic model identification of a micro-air vehicle is proposed. The principal contribution is a technique of wind estimation that provides information about the existing wind during flight when no air-data sensors are available. The estimation technique employs multi-objective optimization algorithms that utilize identification errors to propose the wind-speed components that best fit the dynamic behavior observed. Once the wind speed is estimated, the flight experimentation data are corrected and utilized to perform an identification of the aircraft model parameters. A multi-objective optimization algorithm is also used, but with the objective of estimating the aerodynamic stability and control derivatives. Employing data from different flights offers the possibility of obtaining sets of models that form the Pareto fronts. Deciding which model best adjusts to the experiments performed (compromise model) will be the ultimate task of the control engineer.

---

[1] Teaching and Research Staff, Instituto de Automática e Informática Industrial, Universitat Politècnica de València, jevecar@upv.es.
[2] Teaching and Research Staff, Instituto de Automática e Informática Industrial, Universitat Politècnica de València, sergarro@isa.upv.es.
[3] Teaching and Research Staff, Instituto de Automática e Informática Industrial, Universitat Politècnica de València, jsalcedo@isa.upv.es.
[4] Dean of the College of Engineering, University of South Florida, robertbishop@usf.edu

Nomenclature

b = aircraft wingspan [m]

C_D = drag force coefficient

C_{D_i} = polynomial parameters of the drag coefficient model with $i = \{0, V, \alpha, \alpha^2, q, \delta_e\}$

C_l = torque coefficient in the X direction

C_{l_i} = polynomial parameters of the X aerodynamic moment coefficient model with $i = \{0, \beta, p, r, \delta_a, \delta_r\}$

C_L = lift force coefficient

C_{L_i} = polynomial parameters of the lift coefficient model with $i = \{0, V, \alpha, \alpha^2, \dot{\alpha}, q, \delta_e\}$

C_m = torque coefficient in the Y direction

C_{m_i} = polynomial parameters of the Y aerodynamic moment coefficient model with $i = \{0, V, \alpha, \alpha^2, \dot{\alpha}, q, \delta_e\}$

C_n = torque coefficient in the Z direction

C_{n_i} = polynomial parameters of the Z aerodynamic moment coefficient model with $i = \{0, \beta, p, r, \delta_a, \delta_r\}$

C_X = force coefficient in the X direction

C_Y = force coefficient in the Y direction

C_{Y_i} = polynomial parameters of the Y aerodynamic force coefficient model with $i = \{0, \beta, p, r, \delta_a, \delta_r\}$

C_Z = force coefficient in the Z direction

$\bar{c}$ = aircraft wing chord [m]

$\mathbf{F}$ = resulting force vector acting on aircraft body [N]

$\mathbf{F_A}$ = aerodynamic force vector [N]

$\mathbf{F_G}$ = gravity force vector [N]

$\mathbf{F_T}$ = motor force vector [N]

$F_{\{x,y,z\}}$ = $\{X, Y, Z\}$ components of the resultant force acting on the vehicle and expressed in the body system of reference $\{x_b, y_b, z_b\}$ [N]

g = gravitational field intensity [m/s^2]

I = aircraft tensor of inertia [kg/m^2]

I_p = propeller and rotor set inertia about their rotation axis [kg/m^2]

$I_{\{x,y,z\}}$ = moments of inertia on $\{x_b, y_b, z_b\}$ axes [kg/m^2]

$I_{\{xy,xz,yz\}}$ = products of inertia on x_b, y_b, z_b axes [kg/m^2]

J_i = Cost index for the i^{th} objective

m = aircraft total mass [kg]

$\mathbf{M}$ = resulting moment vector acting on aircraft body [N·m]

$\mathbf{M_A}$ = aerodynamic moment vector [N·m]

$\mathbf{M_T}$ = motor moment vector [N·m]

$M_{\{x,y,z\}}$ = $\{X, Y, Z\}$ components of the resultant moment acting on the vehicle and expressed in the body system of reference $\{x_b, y_b, z_b\}$ [N·m]

N = number of samples in a data set

p = aircraft angular X velocity component respect to ground and expressed in body axes [rad/s]

q = aircraft Y angular velocity component respect to ground and expressed in body axes [rad/s]

$\overline{q}$ = dynamic pressure [Pa]

r = aircraft Z angular velocity component respect to ground and expressed in body axes [rad/s]

S = aircraft aerodynamic surface [m^2]

t_i = i^{th} time instant. $i = 1, 2, ..., N$

T = propeller thrust acting in the direction of its rotation axis [N]

u = aircraft X velocity component respect to ground and expressed in body axes [m/s]

u_{air} = aircraft X velocity component respect to air and expressed in body axes [m/s]

$\mathbf{V}$ = aircraft velocity vector [m/s]

v = aircraft Y velocity component respect to ground and expressed in body axes [m/s]

v_{air} = aircraft Y velocity component respect to air and expressed in body axes [m/s]

V_{air} = aircraft airspeed [m/s]

V_0 = steady state airspeed [m/s]

w = aircraft Z velocity component respect to ground and expressed in body axes [m/s]

w_{air} = aircraft Z velocity component respect to air and expressed in body axes [m/s]

$\mathbf{W}$ = wind velocity vector [m/s]

X^* = unitary scaled value of a variable X

(x_b, y_b, z_b) = aircraft body axes

α = angle of attack [rad]

β = sideslip angle [rad]

δ_a = ailerons deflection [rad]

δ_e = elevators deflection [rad]

δ_r = rudder deflection [rad]

ζ = wind elevation when expressed in spherical coordinates [rad]

θ = aircraft pitch angle [rad]

μ = multi-objective optimization solution

σ = standard deviation of a data set

ϕ = aircraft roll angle [rad]

ξ = wind azimuth when expressed in spherical coordinates [rad]

ψ = aircraft yaw angle [rad]

Ω_p = propeller and rotor rotating speed [rad/s]

I. Introduction

There is an increasingly popular variety of applications that justify the development of unmanned aerial vehicles (UAVs) in the civil aviation field. Possible applications include photography for coastline control and beach erosion tracing, fire detection and control [1], infrastructure inspection, and measurements for agriculture [2]. In this new aeronautics field, high performance at the lowest cost is the main objective.

Several steps towards the achievement of this aim have already been taken. Firstly, it was necessary to reduce the cost and complexity of the aircraft itself. The result was a completely new generation of small airplanes whose size is the minimum necessary to house propulsion, sensorization, and control equipment. Secondly, the integrated systems (sensors, actuators, and control units) had to be powerful enough to control the fast dynamics of these vehicles when completing challenging missions. The cost of such devices is falling thanks to evolution in computer technology. The cost of the development phase has now become an important percentage of the total cost. In addition, hardware integrity is in greater danger during this phase. Therefore, a minimization of the total number of test hours is desired. Making use of simulation tools and utilizing acquired data as much as possible can lower development costs and risks. Thus, obtaining a dynamic model that

tightly adjusts to the real flight behavior of the aircraft is essential for obtaining precise simulation results and correctly designing control algorithms. The process of going from observed data to a mathematical model is fundamental in science and engineering. In system theory, this process is known as system identification and the objective is to obtain dynamic models from observed input and output signals [3]. In particular, system identification methods have been used for flight-test evaluations [4–10], control analysis and design [11, 12] and advanced simulation [13–15].

Identifying the aerodynamic model of a low-cost micro-air vehicle (MAV) is a major challenge. Generally, wind tunnel tests are too expensive to be driven, and experimental flight data has to be used instead. In addition, this type of aircraft usually has a light body and flies slowly, meaning that the slightest breeze contributes significantly to overall airspeed. Hence, the information available from the inertial sensors is insufficient [16–18] for the identification of their aerodynamic model. In [19–21], different wind estimation techniques are presented. Those works make use of an extended Kalman filter to fuse inertial information with external sensors, such as pitot tubes or optical flow sensors. However, due to lack of space and resources air-data sensors may be unavailable or highly inaccurate in some occasions. Designing control strategies in these cases becomes a hard process, since there is no trustworthy model.

To improve a situation in which no air-data sensor is available, a two step identification methodology based on multi-objective optimization (MO) is presented in this paper. The methodology makes use of flight data instead of wind tunnel experiments to identify the non-dimensional stability and control derivatives of a micro-air vehicle. As the main contribution, our methodology starts with a wind estimation technique that complements the information collected by the inertial sensors. This technique takes information from the inertial unit, the global positioning system (GPS) sensor, and the control inputs to estimate the wind that best fits a given model structure. The quality of the identified models is consequently improved and no additional air-data sensor is used for that purpose. Model identification is performed in a second step. The identification technique also relies on the advantages offered by an MO perspective, enabling the designer to test flight data from different types of experiments. Thereby, models with acceptable performance in various realistic flight regimes are obtained.

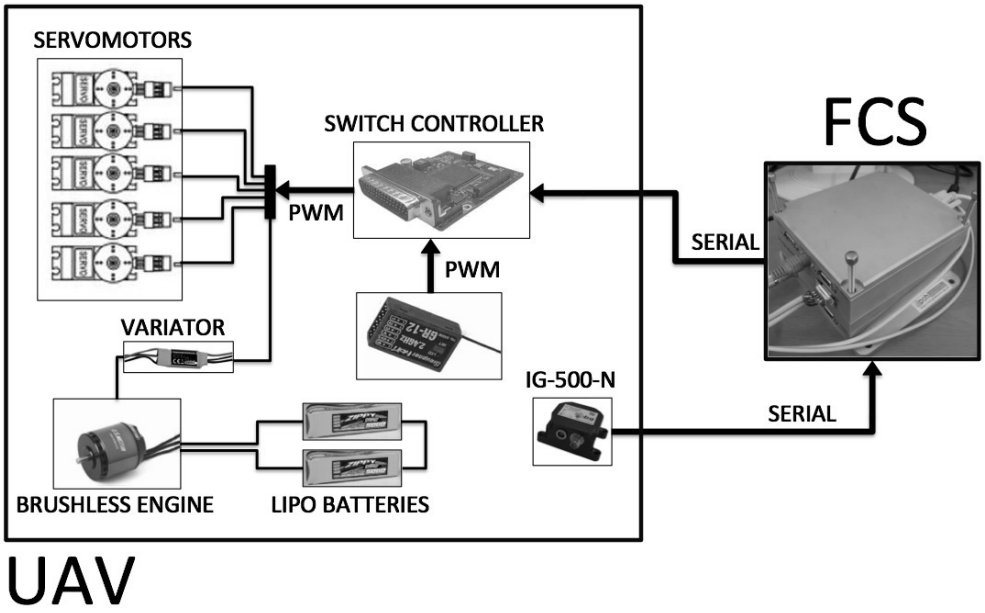

Fig. 1: Interconnection between the UAV devices and the flight control system

The paper is organized as follows. Section II introduces the aircraft and the hardware used in the experiments along with the dynamic and aerodynamic models. In Section III, the estimation procedure is presented and developed. Section IV provides a step-by-step explanation of how to obtain the final parameters of the aerodynamic models once the data has been corrected. The results are divided in two sections. Section V presents simulation results that verify the validity of the wind estimation technique. Section VI presents results for both the estimation and identification tasks. Section VII presents the final conclusions.

II. UAV Testbench

A. Flight System

The main component of the UAV flight system is a Kadett 2400 aircraft manufactured by Graupner. The aircraft has a very lightweight frame and characteristics that make it suitable for the purposes of this research. These characteristics include a 2.4 m wing span, 0.9 m^2 of wing surface, 48.07 N/m^2 wing loading, and 1.65×10^{-2} m^3 of available volume to house control hardware.

Figure 1 illustrates interconnection between the UAV devices and the flight control system. The aircraft houses all the devices necessary for manual, as well as automatic, control. During

Table 1: IG500N unit characteristics

Sensor	Characteristic	Value
Unit attitude		
	Static accuracy (Pitch)	±0.5 deg
	Static accuracy (Roll)	±0.5 deg
	Static accuracy (Heading)	±1.0 deg
	Dynamic accuracy	±1.0 deg rms
Accelerometers		
	Non-linearity	< 0.2 % of full scale
	Bias stability	±5 mg
Gyroscopes		
	Non-linearity	< 0.1 % of full scale
	Bias stability	±0.5 deg/s
Magnetometers		
	Non-linearity	< 0.2 % of full scale
	Bias stability	±0.5 mG
GPS Receiver		
	Horizontal accuracy	2.0 m
	Vertical accuracy	5.0 m

normal flight, the tail rudder, elevators, and ailerons serve as the control surfaces. Propulsion is provided by a brushless alternating current engine supplied by two lithium-ion polymer (LiPo) batteries through a frequency variator. The variator and the servomotors are controlled by pulse width modulated (PWM) command signals. The servo switch controller (SSC) switches between manual and autonomous flight modes. It also enables data acquisition and the application of control surface deflections and motor torque changes.

The flight control station (FCS), housed in a PC-104, hosts the control algorithms. The control loop is closed by a IG500N unit from SBG Systems, that integrates a wide range of sensors, including the accelerometers, gyroscopes, and magnetometers. A Kalman filter fuses the sensor information

to estimate the position, orientation, linear and angular speed, and acceleration. Table 1 provides manufacturer's accuracy data for the IG500N unit. This same platform was presented in [22–25] together with the results of the first flight tests.

B. Aircraft Dynamic Model

As stated in [26], the aircraft dynamic model is given by the force equations,

$$\begin{aligned}
\dot{u} &= rv - qw + \frac{\overline{q}S}{m}C_X(\delta_{[e,a,r]}) - g\sin\theta + \frac{T}{m} \\
\dot{v} &= pw - ru + \frac{\overline{q}S}{m}C_Y(\delta_{[e,a,r]}) + g\cos\theta\sin\phi \\
\dot{w} &= qu - pv + \frac{\overline{q}S}{m}C_Z(\delta_{[e,a,r]}) + g\cos\theta\cos\phi
\end{aligned} \tag{1}$$

, torque equations,

$$\begin{aligned}
\dot{p} - \frac{I_{xz}}{I_x}\dot{r} &= \frac{\overline{q}Sb}{I_x}C_l(\delta_{[e,a,r]}) - \frac{I_z - I_y}{I_x}qr + \frac{I_{xz}}{I_x}qp \\
\dot{q} &= \frac{\overline{q}S\overline{c}}{I_y}C_m(\delta_{[e,a,r]}) - \frac{I_x - Iz}{I_y}pr - \frac{I_{xz}}{I_y}(p^2 - r^2) + I_p\Omega_p r \\
\dot{r} - \frac{I_{xz}}{I_z}\dot{p} &= \frac{\overline{q}Sb}{I_z}C_n(\delta_{[e,a,r]}) - \frac{I_y - I_x}{I_z}pq - \frac{I_{xz}}{I_z}qr - I_p\Omega_p q
\end{aligned} \tag{2}$$

and kinematic equations,

$$\begin{aligned}
\dot{\phi} &= p + \tan\theta(q\sin\phi + r\cos\phi) \\
\dot{\theta} &= q\cos\phi - r\sin\phi \\
\dot{\psi} &= \frac{q\sin\phi + r\cos\phi}{\cos\theta}
\end{aligned} \tag{3}$$

In Eq. 1, Eq. 2 and Eq. 3 g is the gravitational field intensity near the Earth's surface, and m is the total mass of the system. Given the body reference frame $X_bY_bZ_b$ illustrated in Fig. 2, (u, v, w) are the components of the translational velocity, (p, q, r) the components of the angular velocity, (I_x, I_y, I_z) are the moments of inertia, and I_{xz} is a product of inertia. The products of inertia I_{xy} and I_{yz}, related to the longitudinal plane ($Y_b = 0$), are both null because of the aircraft's symmetry

with respect to this plane. I_p is the rotating inertia of the tandem motor and propeller, Ω_p is its rotating speed, and T is the motor thrust. S, b and $\overline{c}$ are the the Kadett 2400 aerodynamic surfaces, wingspan, and wing chord respectively, and $\overline{q}$ is the dynamic pressure, which is a function of the air density and airspeed relative to the local wind. The aerodynamic coefficients (AC) C_X, C_Y, C_Z, C_l, C_m, and C_n, are functions of the system variables. In particular, the δ symbol in brackets represents its dependency on the deflections of the control surfaces (δ_e, δ_a and δ_r are the elevators, ailerons, and rudder deflections respectively). The aerodynamic coefficients will be presented in further detail in Section II C. Finally, the aircraft orientation is represented by the Euler angles of roll ϕ, pitch θ, and yaw ψ.

C. Aircraft Aerodynamic Model

In Klein and Morelli [26], detailed information on the aerodynamic coefficients is provided. Firstly, if we assume a scenario in which the aircraft is in steady flight, and only performs short manoeuvres that begin from this state, we can truncate the Taylor series expansion and retain only the first or second-order terms. Furthermore, under the assumption of small perturbations, and based on the symmetry of the vehicle, it can be assumed that: 1) the symmetrical (longitudinal) variables u, w and q do not affect asymmetrical (lateral) force and torques; and similarly, 2) asymmetric (lateral) variables v, p and r do not affect the symmetrical (longitudinal) forces and torque. The aerodynamic coefficients are given by the longitudinal aerodynamic models,

$$\begin{aligned}
C_D =& C_{D_0} + C_{D_{V_{air}}} \frac{1}{V_0} \Delta V_{air} + C_{D_\alpha} \Delta\alpha + C_{D_{\alpha^2}} \Delta\alpha^2 + C_{D_q} \frac{\overline{c}}{2V_0} q + C_{D_{\delta_e}} \Delta\delta_e \\
C_L =& C_{L_0} + C_{L_{V_{air}}} \frac{1}{V_0} \Delta V_{air} + C_{L_\alpha} \Delta\alpha + C_{L_{\alpha^2}} \Delta\alpha^2 + C_{L_{\dot\alpha}} \frac{\overline{c}}{2V_0} \dot\alpha + C_{L_q} \frac{\overline{c}}{2V_0} q + C_{L_{\delta_e}} \Delta\delta_e \\
C_m =& C_{m_0} + C_{m_{V_{air}}} \frac{1}{V_0} \Delta V_{air} + C_{m_\alpha} \Delta\alpha + C_{m_{\alpha^2}} \Delta\alpha^2 + C_{m_{\dot\alpha}} \frac{\overline{c}}{2V_0} \dot\alpha + C_{m_q} \frac{\overline{c}}{2V_0} q + C_{m_{\delta_e}} \Delta\delta_e
\end{aligned} \tag{4}$$

and the lateral aerodynamic models,

$$\begin{aligned}
C_Y =& C_{Y_0} + C_{Y_\beta} \Delta\beta + C_{Y_p} \frac{b}{2V_0} p + C_{Y_r} \frac{b}{2V_0} r + C_{Y_{\delta_a}} \Delta\delta_a + C_{Y_{\delta_r}} \Delta\delta_r \\
C_l =& C_{l_0} + C_{l_\beta} \Delta\beta + C_{l_p} \frac{b}{2V_0} p + C_{l_r} \frac{b}{2V_0} r + C_{l_{\delta_a}} \Delta\delta_a + C_{l_{\delta_r}} \Delta\delta_r \\
C_n =& C_{n_0} + C_{n_\beta} \Delta\beta + C_{n_p} \frac{b}{2V_0} p + C_{n_r} \frac{b}{2V_0} r + C_{n_{\delta_a}} \Delta\delta_a + C_{n_{\delta_r}} \Delta\delta_r
\end{aligned} \tag{5}$$

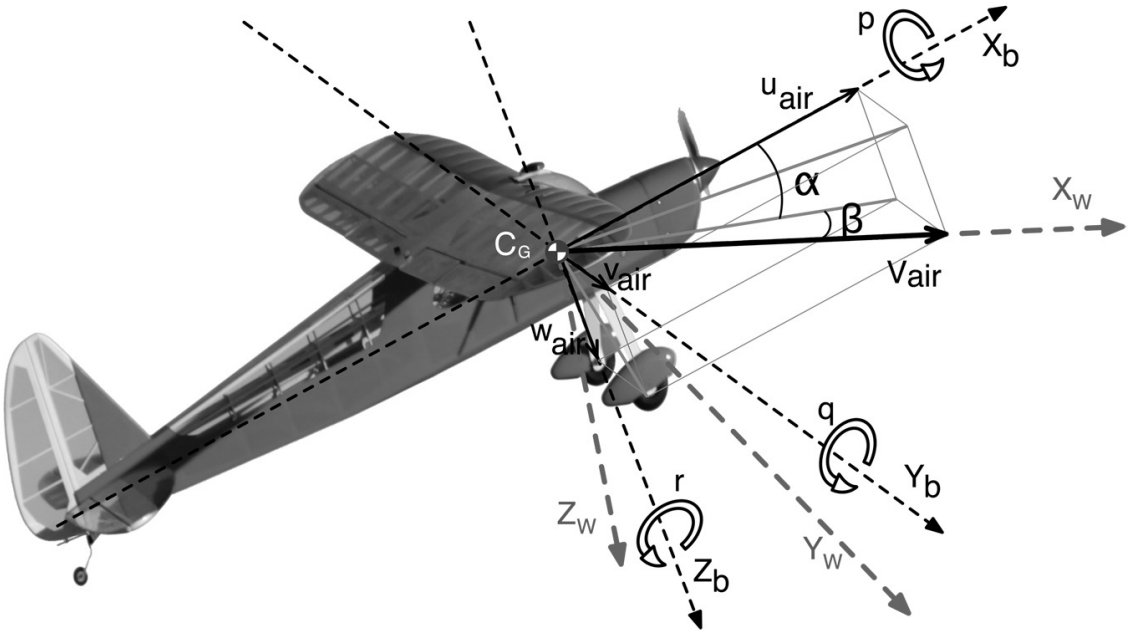

Fig. 2: Aircraft body axes, aircraft wind axes, and wind relative velocity

where α and β are the angle of attack and of sideslip, respectively, and V_{air} is the airspeed (see Fig. 2). In particular, V_0 is airspeed measured at the steady state of flight, before a manoeuvre begins. These variables are velocity dependent and calculated as:

$$\alpha = \arctan\left(\frac{w_{air}}{u_{air}}\right); \quad \text{and} \quad \beta = \arcsin\left(\frac{v_{air}}{V_{air}}\right); \tag{6}$$

where $V_{air} = |\mathbf{V_{air}}|$. As denoted in Fig. 2, u_{air}, v_{air} and w_{air} are the three components of the aircraft velocity with respect to air. Under zero-wind conditions $(u_{air}, v_{air}, w_{air}) = (u, v, w)$. Finally, C_L and C_D are the lift and drag coefficients and their relation to C_X and C_Z is:

$$C_L = -C_Z \cos\alpha + C_X \sin\alpha; \quad \text{and} \quad C_D = -C_X \cos\alpha - C_Z \sin\alpha; \tag{7}$$

Thus, the aerodynamic model identification is based on extracting the constants of the polynomials of Eq. (4) and (5) from the flight data and by means of the dynamic model. Those constants are called non-dimensional stability and control derivatives.

III. Wind Estimation Technique

A. Methodology Outline

MAVs are generally unable to carry precise airspeed sensors that provide three-dimensional data needed for correct identification of the aerodynamic model. In the case of the platform presented in this paper, a GPS and an inertial-magnetic unit (IMU) supply a reasonably good estimate of the velocities relative to the Earth's surface, but do not provide information about the velocities relative to air. To improve the identified stability and control derivatives, a wind estimation methodology is incorporated into the procedure of parameter identification. The estimation methodology is based on the fact that, for small airplanes, which fly at relatively low airspeeds, the smallest breeze may be a large percentage of the total airspeed value, thus introducing a large error if not taken into account. Hence, assuming the model structure is well defined, an optimization problem can be posed in which a three-component solution (wind) is searched to minimize the error of a particular aerodynamic coefficient model.

It will be shown in the following sections that longitudinal or lateral experiments can be used to obtain all the coefficient models. This means that a total number of three models per experiment can be derived. Therefore, the aforementioned optimization becomes a particular multi-objective optimization problem in which a unique solution should be obtained if the actual wind is found. In practice, a cloud of solutions close to the real wind will be obtained by the optimizer.

B. Multi-objective Optimization

In engineering problems, it is a common issue to deal with situations that require the optimization of multiple objectives that include physical constraints, operational constraints, and non-linearities. Due to this fact, addressing these problems from the standpoint of classical optimization is insufficient [27]. The multi-objective optimization problem (MOP) can be stated as:

$$\min_{\mu \in \mathbb{R}} J(\mu) = [J_1(\mu), J_2(\mu), \ldots, J_m(\mu)] \tag{8}$$

where μ is the solution that minimizes the m cost functions J_i at the same time. Generally, it will not be possible to find a solution that satisfies all requirements at once, so the optimizer will

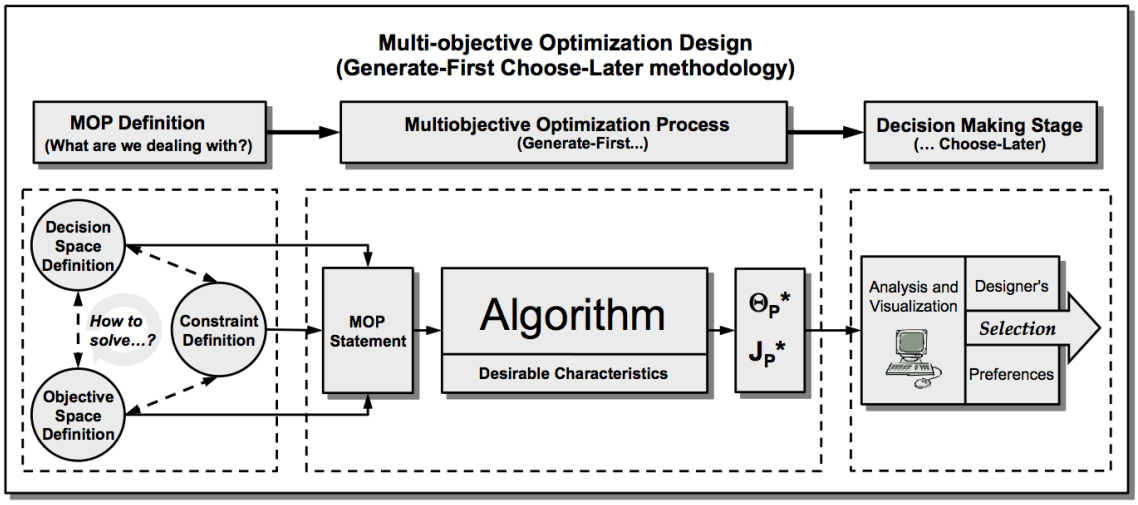

Fig. 3: Multi-objective Optimization Design (MOOD) [29]

have to provide the set of solutions that are not improved by any other set in all the objectives simultaneously. That set of solutions is known as the Pareto set Θ^*, and their values in the objective space create the Pareto front J_p^*.

Definition 1. ***(Pareto optimality [28])****: An objective vector $J(\mu_1)$ is Pareto optimal if there is no other objective vector $J(\mu_2)$ such that $J_i(\mu_2) \leq J_i(\mu_1)$ for all $i \in [1, 2, \ldots, m]$ and $J_j(\mu_2) < J_j(\mu_1)$ for at least one $j, j \in [1, 2, \ldots, m]$.*

Definition 2. ***(Strict Dominance [28])****: An objective vector $J(\mu_1)$ is dominated by another objective vector $J(\mu_2)$ if $J_i(\mu_2) < J_i(\mu_1)$ for all $i \in [1, 2, \ldots, m]$.*

Definition 3. ***(Dominance [28])****: An objective vector $J(\mu_1)$ dominates another vector $J(\mu_2)$ if $J(\mu_1)$ is not worse than $J(\mu_2)$ in all objectives and is better in at least one objective; that is $J(\mu_1) \prec J(\mu_2)$*

Figure 3 illustrates how MO is employed as a design methodology. Three stages comprise the procedure: MOP definition; a multi-objective optimization process; and decision making [30]. The technique must be viewed as a holistic process in which equal importance is assigned to each stage so that the design process is successfully driven [31]. Hence, objective and decision spaces and their constraints must be well defined in the MOP definition stage so that the correct problem is optimized in the optimization process. Finally, a deep analysis should be carried out (once an approximation

to the Pareto front is available) to detect the most convenient solution in the decision making stage. This same topology is followed in the wind estimation process.

1. MOP Definition

An aircraft is a complex system with multiple control inputs that simultaneously excite multiple state variables. As already mentioned, the aerodynamic coefficients depend on the inputs and state variables. If an experiment is performed in which a longitudinal input is altered by collecting the longitudinal variable values then any coefficient of this type can be modeled. Thus, elevator deflection and motor thrust variations (which generate changes in the longitudinal variables) can be used to model any longitudinal coefficient and, in the same way, ailerons and rudder deflections can be used to model lateral coefficients. Experiments in which elevators or motors are moved from their setpoints will be denoted as longitudinal experiments, and similarly, experiments in which the tail rudder or ailerons are moved from their setpoints will be denoted as lateral experiments.

For the purpose of the wind estimation problem as proposed here, the methodology is reinforced by the fact that at least three models can be extracted from the same data set. Indeed, if the correct wind is estimated, estimation errors for all coefficient models will decrease simultaneously. From a different standpoint, if a solution in the wind components that minimizes the error of the three coefficient models at the same time is found, it is probable that this solution is the actual wind experienced during the flight experiment.

Short time experiments are performed and utilized in the wind estimation and identification process. Test duration is an important question because it directly affects the wind estimation process. Bidirectional input-step experiments were made with the minimum time required so that the assumption of constant wind remains reasonable. Three constant wind components are then used as an approximation of the wind along each experiment. Three objectives are defined, one per aerodynamic coefficient model. If the MSE is used as the performance index of the identification process, three cost functions can be defined for each experiment. The three longitudinal cost functions are:

$$
\begin{aligned}
J_1(\mathbf{W}) =& \frac{1}{N}\sum_{h=1}^{N}\Big[C_D(t_h,\mathbf{W},\cdots)-\hat{C}_D(t_h,\mathbf{W},\cdots)\Big]^2\\
J_2(\mathbf{W}) =& \frac{1}{N}\sum_{h=1}^{N}\Big[C_L(t_h,\mathbf{W},\cdots)-\hat{C}_L(t_h,\mathbf{W},\cdots)\Big]^2\\
J_3(\mathbf{W}) =& \frac{1}{N}\sum_{h=1}^{N}\Big[C_m(t_h,\mathbf{W},\cdots)-\hat{C}_m(t_h,\mathbf{W},\cdots)\Big]^2
\end{aligned}
\tag{9}
$$

Similarly, the lateral cost functions are:

$$
\begin{aligned}
J_1(\mathbf{W}) =& \frac{1}{N}\sum_{h=1}^{N}\Big[C_Y(t_h,\mathbf{W},\cdots)-\hat{C}_Y(t_h,\mathbf{W},\cdots)\Big]^2\\
J_2(\mathbf{W}) =& \frac{1}{N}\sum_{h=1}^{N}\Big[C_l(t_h,\mathbf{W},\cdots)-\hat{C}_l(t_h,\mathbf{W},\cdots)\Big]^2\\
J_3(\mathbf{W}) =& \frac{1}{N}\sum_{h=1}^{N}\Big[C_n(t_h,\mathbf{W},\cdots)-\hat{C}_n(t_h,\mathbf{W},\cdots)\Big]^2
\end{aligned}
\tag{10}
$$

In Eq. 9 and Eq. 10 $\hat{C}_D$, $\hat{C}_L$, $\hat{C}_m$, $\hat{C}_Y$, $\hat{C}_l$, and $\hat{C}_n$ are the values that the identified coefficient models provide for C_D, C_L, C_m, C_Y, C_l, and C_n, respectively. These cost functions constitute the objective space while the three possible wind components define the decision space. In this paper, the wind speed is expressed in spherical coordinates with the vector magnitude $|\mathbf{W}|$ as the radius, and the two rotation angles, elevation, denoted by ζ, and azimuth, denoted by ξ; giving the triple $\mathbf{W} = (|\mathbf{W}|, \zeta, \xi)$. With the aim of unequivocally defining the decision space, the radius, the elevation, and the azimuth should be enclosed into three intervals consistent with the cost functions domain. The space definition of this interval in this paper is:

$$
D_{(J)} = \{(|\mathbf{W}|, \zeta, \xi) : |\mathbf{W}| \in [0, +\infty[\,, \zeta \in [-\pi/2, \pi/2]\,, \xi \in [0, 2\pi[\}
\tag{11}
$$

Finally, constraints may be included in the objectives, as well as in the decision variables. In this work, constraints have been introduced only in the decision space in order to narrow the space of possible solutions. Such a narrowing has been performed based on knowledge about the maximum magnitude of the wind speed during the day of the flight experiments.

2. Multi-objective Optimization Process

Extensive literature exists about how multi-objective optimization problems can be solved. Some of the classical strategies to approximate the Pareto set include: normal constraint method [32, 33], normal boundary intersection (NBI) method [34], epsilon constraint techniques [28] and physical programming [35]. Multi-objective evolutionary algorithms (MOEA) have been used to approximate a Pareto set [36], due to their flexibility when evolving an entire population towards the Pareto front. A comprehensive review of the early stages of MOEAs is contained in [37]. There are several popular evolutionary and nature-inspired techniques used by MOEAs. The most popular techniques include genetic algorithms (GA) [38, 39], particle swarm optimization (PSO) [40, 41], and differential evolution (DE) [42–44]. Nevertheless, evolutionary techniques such as artificial bee colony (ABC) [45] or ant colony optimization (ACO) [46] algorithms are becoming popular. No evolutionary technique is better than the others, since all have drawbacks and advantages. These evolutionary/nature-inspired techniques require mechanisms to deal with evolutionary multi-objective optimization (EMO) since they were originally used for single-objective optimization. While the dominance criterion (definition 3) could be used to evolve the population towards a Pareto front, it could be insufficient to achieve a minimum degree of satisfaction in other desirable characteristics for a MOEA (diversity, for instance)[47].

The authors of this paper have taken part in the development of a MOEA called the spMODE algorithm [48, 49]. It is a heuristic algorithm that makes use of the convergence properties of evolution to approximate the Pareto front. It uses physical programming to incorporate the designer's preferences, size control of the approximated Pareto front, as well as spherical pruning to improve spreading. Hence it is a MOEA with mechanisms to improve and deal with diversity, pertinency, many-objective optimization instances, and constrained optimization instances. Although spMODE has been chosen to solve this MOP, any other multi-objective optimizer could be used for this purpose.

Since an evolution algorithm is used, multiple wind candidates are proposed in each generation by the optimizer and all are then evaluated. Figure 4 illustrates the routine followed by the optimizer. Starting from a given wind-speed, the airspeed denoted by $\mathbf{V_{air}}$ is calculated as:

$$\mathbf{V_{air}} = \mathbf{V_{GPS}} - \mathbf{W} \tag{12}$$

where $\mathbf{V_{GPS}}$ denotes the aircraft velocity relative to the Earth's surface. Note that $\overline{q}$ is dependent on $\mathbf{V_{air}}$. Once the aircraft velocity relative to air is available, the airspeed dependent variables on the right side of the aircraft aerodynamic model (in Eqs. (4) and (5)) can be obtained. Furthermore, as the aerodynamic coefficients cannot be measured directly, dynamic expressions must be used for the purpose of estimating their values. These relationships are given by [26]:

$$\begin{aligned}
C_X =& \frac{1}{\overline{q}S}(ma_x - T) \\
C_Y =& \frac{ma_y}{\overline{q}S} \\
C_Z =& \frac{ma_z}{\overline{q}S} \\
C_l =& \frac{1}{\overline{q}Sb}\left[I_x\dot{p} - I_{xz}\left(pq + \dot{r}\right) + \left(I_z - I_y\right)qr\right] \\
C_m =& \frac{1}{\overline{q}S\overline{c}}\left[I_y\dot{q} + \left(I_x - I_z\right)pr + I_{xz}\left(p^2 - r^2\right) - I_p\Omega_p r\right] \\
C_n =& \frac{1}{\overline{q}Sb}\left[I_z\dot{r} - I_{xz}\left(\dot{p} - qr\right) + \left(I_y - I_x\right)pq + I_p\Omega_p q\right]
\end{aligned} \tag{13}$$

Note that $\overline{q}$ is present in each realtionship of Eq.(13). This means that the aerodynamic coefficients are directly dependent on airspeed and thus, on the wind during data recollection. Due to this fact, recalculation of the aerodynamic coefficients is carried out in each evaluation performed by the MOEA.

The next step is the cost calculation. After calculating the airspeed dependent variables, the aerodynamic coefficients and the regressors are scaled according to their standard deviations. The scaling expression is:

$$X^* = \frac{X - X_0}{\sqrt{N}\sigma(X)} \tag{14}$$

where X represents any of those airspeed dependent variables, X^* is its value after being scaled by applying Eq. (14), and N and $\sigma(X)$ are the number of samples and the standard deviation of

X during the experiment, respectively. This strategy is often followed in regression analysis of a multivariate distribution to overcome the problem of variances of the residuals changing at different input variable values [50]. Since we are recalculating the estimated variables C_i at each iteration and they are directly proportional to V_{air}^{-2} (given that $\overline{q} = 1/2\rho V_{air}^2$), this scaling makes the estimation error independent of the velocity's magnitude. After scaling, the least-squares method is applied to obtain three longitudinal auxiliary models,

$$\begin{aligned} C_D^* =& C_{D_{V^*}} V^* + C_{D_{\alpha^*}} \alpha^* + C_{D_{(\alpha^2)^*}} (\alpha^2)^* + C_{D_{q^*}} q^* + C_{D_{\delta_e^*}} \delta_e^* \\ C_L^* =& C_{L_{V^*}} V^* + C_{L_{\alpha^*}} \alpha^* + C_{L_{(\alpha^2)^*}} (\alpha^2)^* + C_{L_{\dot{\alpha}^*}} \dot{\alpha}^* + C_{L_{q^*}} q^* + C_{L_{\delta_e^*}} \delta_e^* \\ C_m^* =& C_{m_{V^*}} V^* + C_{m_{\alpha^*}} \alpha^* + C_{m_{(\alpha^2)^*}} (\alpha^2)^* + C_{m_{\dot{\alpha}^*}} \dot{\alpha}^* + C_{m_{q^*}} q^* + C_{m_{\delta_e^*}} \delta_e^* \end{aligned} \tag{15}$$

or three lateral auxiliary models

$$\begin{aligned} C_Y^* =& C_{Y_{\beta^*}} \beta^* + C_{Y_{p^*}} p^* + C_{Y_{r^*}} r^* + C_{Y_{\delta_a^*}} \delta_a^* + C_{Y_{\delta_r^*}} \delta_r^* \\ C_l^* =& C_{l_{\beta^*}} \beta^* + C_{l_{p^*}} p^* + C_{l_{r^*}} r^* + C_{l_{\delta_a^*}} \delta_a^* + C_{l_{\delta_r^*}} \delta_r^* \\ C_n^* =& C_{n_{\beta^*}} \beta^* + C_{n_{p^*}} p^* + C_{n_{r^*}} r^* + C_{n_{\delta_a^*}} \delta_a^* + C_{n_{\delta_r^*}} \delta_r^* \end{aligned} \tag{16}$$

Note that these models are utilized to acquire a value of the fitting goodness and do not represent the actual behavior of the aerodynamic coefficients. Identifying the real models is accomplished after estimating the wind and correcting the experimental data.

Once these auxiliary models are available, the MSE is computed and with it, the value of three cost functions. Finally, if the currently evaluated wind is a non-dominated solution, it is added as part of the Pareto front approximation. Otherwise, it is discarded as a solution, though used as valuable information in the evolution process (see Fig. 4).

3. Decision Making Stage

A unique wind must be chosen. Acknowledging that this technique is not being used for design but for estimating, a best solution does exist that is factually and independent of the designer's preferences. The question is, does the estimate accurately represent the wind? To address that key

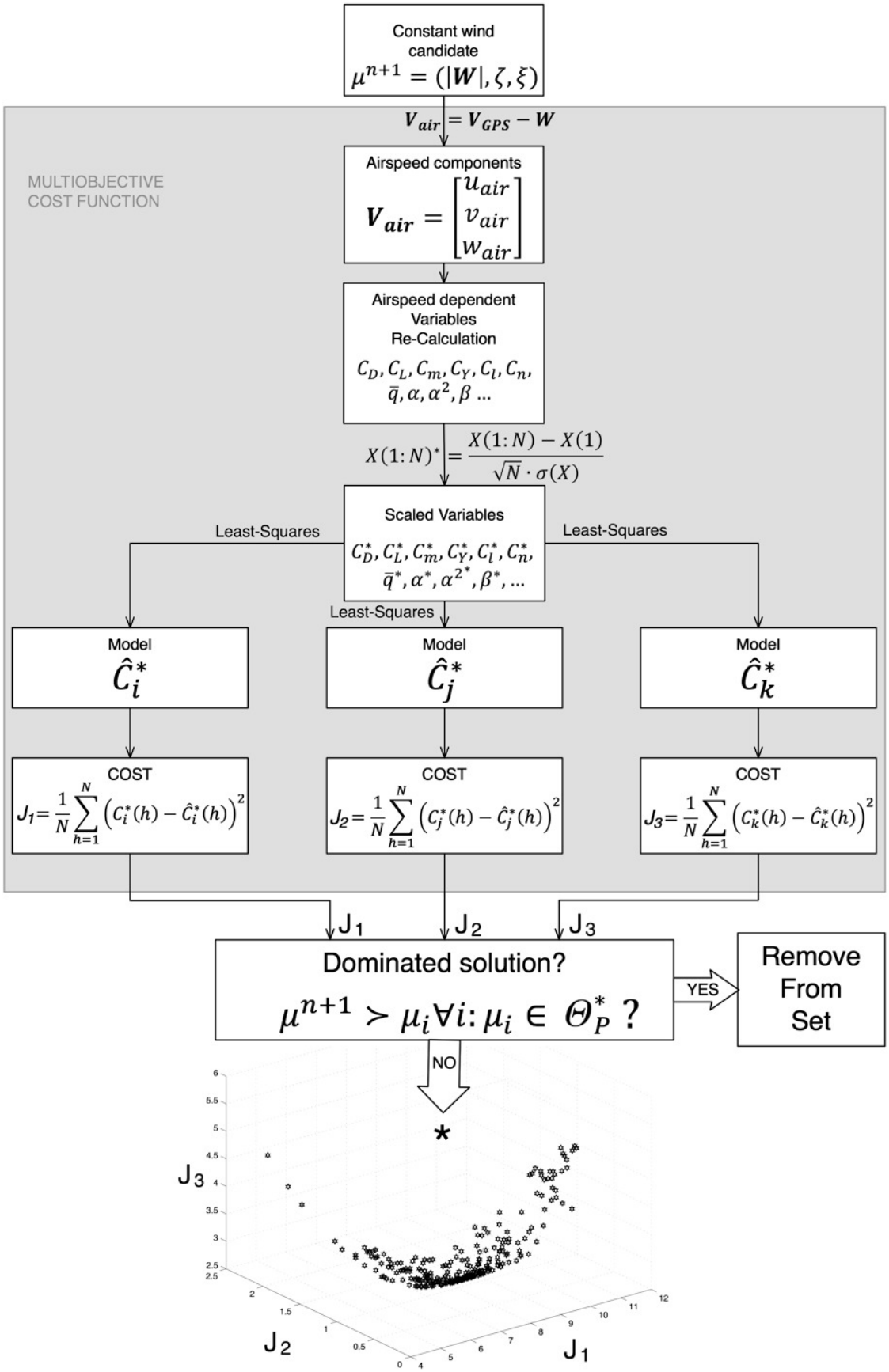

Fig. 4: Wind estimation process

question, the following two-step validation process is proposed:

1. Firstly, a 3D representation of the whole set of wind vectors (set of solutions given by the optimizer) is obtained. If that set is concentrated around a given point, then this is likely a good estimation of the wind speed. On the contrary, if the set of solutions is scattered or concentrated at multiple points, then there is not a unique global minimum and, therefore, the estimation process was unsuccessful.

2. Secondly, if the first step led to the conclusion of a successful estimation, this fact may still be refuted or confirmed with a set of validation data. The way to proceed is:

   (a) Perform a least-squares identification with two sets of data. This will result in two models for each of the aerodynamic coefficients. Note that the estimated wind is not yet used.

   (b) Perform a cross validation for each of the models obtained in 2a. This is, taking a model identified with set 1, compute its MSE for set 2 and *vice versa*.

   (c) Correct each set of data with the estimated wind, recalculating airspeed and all airspeed dependent variables accordingly.

   (d) As in 2a, use the least-squares method to identify the aerodynamic coefficient models that best fit each set of treated data. Note that unlike step 2a, this time the estimated wind has been used to correct the data.

   (e) Perform a cross validation of the models identified in 2d, to obtain their fitting errors. If validation errors are now smaller than the ones obtained in step 2b, then the wind speeds were successfully estimated. Otherwise, the minimums found by the algorithm are not the wind speeds acting during the experiments.

IV. Aerodynamic Model Identification

A methodology based on least-squares is commonly used for modeling aerodynamic coefficients. When multiple inputs excite the variables of one model, considerations such as coordination, correlation, and relative effectiveness appear. In [51] the authors give detailed information about how to design experiments for aerodynamic model identification with multiple inputs involved. Optimally

designed time-skewed doublet inputs seem to be a good option in these cases. However, conducting optimal experiments becomes impossible for a pilot controlling the aircraft from earth, as in the case of MAVs. A problem of experiment effectiveness appears because when time-skewed doublet inputs are used, the duration of each experiment determines its weight in the optimization process. For this reason, a multi-objective optimization is proposed here for the aerodynamic model identification of an MAV. Multi-objective techniques applied to model identification have achieved very good results in many cases, as shown in [52–54]. When the optimization problem turns out to be non-convex, there exist solutions in the Pareto set that remain unreachable for a weighted-sum method. Figure 5 shows a non-convex Pareto front and how the straight lines resulting from the different combination of objectives weights are unable to reach part of the Pareto front. Thus, optimizing objectives separately present a great advantage when non-convex problems must be solved. Several additional advantages derive from an MO perspective applied to this particular problem. Firstly, the weights of each type of experiment can be determined *a posteriori*. Secondly, flight conditions do not depend on the previous experiment. Thirdly, metrics other than mean squared error (MSE) can be used in the optimization. And lastly, the duration of the experiments is reduced. The latter favors our wind estimation process because the constant wind assumption weakens as the durations of the experiments increase.

Thus, the second part of this work is the estimation of the aerodynamic model that describes how the MAV reacts to changes in control inputs. As mentioned, an accurate MAV model cannot be obtained without taking wind disturbances into account. For that purpose a process of wind estimation was detailed in the previous section and now an aerodynamic model identification that makes use of the wind information is needed. Once information about the estimated wind acting during tests is available, variables affected by the relative airspeed may be corrected. The relative velocity vector is computed in first place, and then the angle of attack α and the sideslip angle β are estimated by means of Eq. (6).

As stated, longitudinal and lateral experiments, independently excite different sets of aerodynamic coefficients. Four different experiments can be performed to excite the longitudinal and lateral aerodynamic coefficients. Elevator deflections and motor thrust variations, generate changes in the

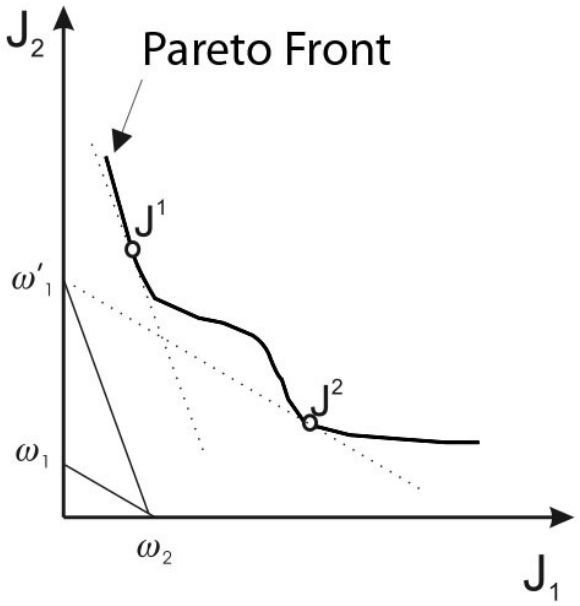

Fig. 5: Pareto front approximation by weighted-sum technique

longitudinal variables and, aileron and rudder deflections generate changes in the lateral variables. Therefore, longitudinal and lateral coefficient models can be identified from different type of experiments. As an example, if a C_D model is obtained by optimizing an elevator deflection test, the model performance on motor experiment data will decrease, and *vice versa*. So, an identification process that takes both experiments into account simultaneously is a bi-objective optimization problem.

Figure 6 has been included to illustrate the bi-objective optimization concept. If the MSE is again used as the performance index of the identification process, two cost functions can be defined for each aerodynamic coefficient. The two cost functions used for obtaining any of the longitudinal models are:

$$J_1 = \frac{1}{N_{elevator}} \sum_{i=1}^{N_{elevator}} \left[C_j(t_i) - \hat{C}_j(t_i) \right]^2 \qquad \forall j \in \{D, L, m\} \tag{17}$$

$$J_2 = \frac{1}{N_{motor}} \sum_{i=1}^{N_{motor}} \left[C_j(t_i) - \hat{C}_j(t_i) \right]^2 \qquad \forall j \in \{D, L, m\} \tag{18}$$

where $\hat{C}_j(t_i)$ is the model approximation of the C_j value at the instant t_i and $N_{elevator}$ and N_{motor} are the number of samples of each type of experiment. Similar cost functions can be defined for the three lateral models.

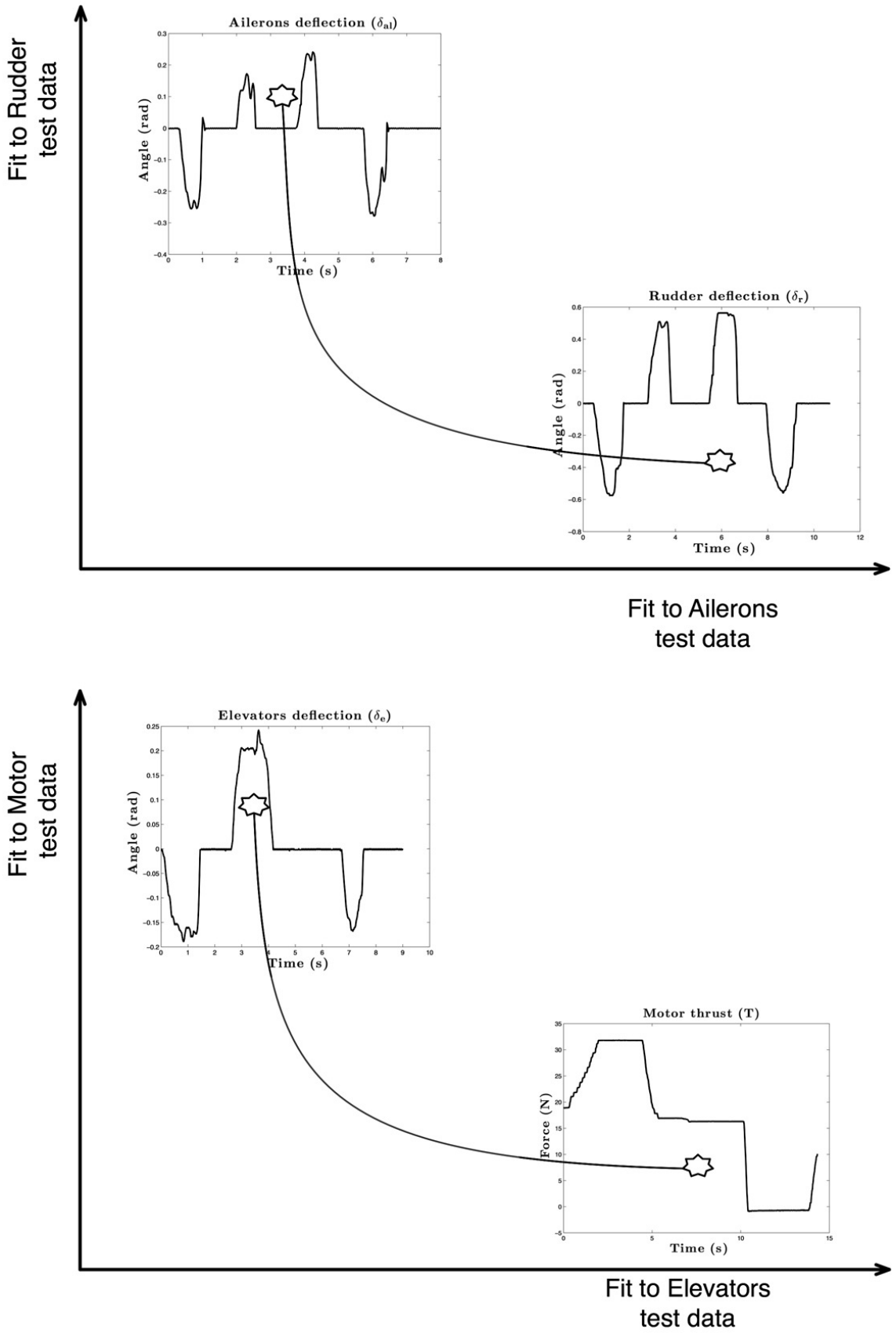

Fig. 6: Bi-objective optimization identification concept

Then, if C_l is to be modeled using aileron and rudder experiments, the identification problem from this MO point of view should be stated as

$$\min_{\mu\in\mathbb{R}^6}\left(\frac{1}{N_{ailerons}}\sum_{i=1}^{N_{ailerons}}\left[C_l(t_i)-\hat{C}_l(t_i,\mu)\right]^2,\frac{1}{N_{rudder}}\sum_{i=1}^{N_{rudder}}\left[C_l(t_i)-\hat{C}_l(t_i,\mu)\right]^2\right) \tag{19}$$

where $\mu = \left[C_{l_0}, C_{l_\beta}, C_{l_p}, C_{l_r}, C_{l_{\delta_a}}, C_{l_{\delta_r}}\right]$. A total of six full optimization processes are required to obtain the complete set of solutions for the aerodynamic model. A decision making stage will complete the methodology. In that stage, exhaustive analysis of the aircraft behavior in the different tests must be made to determine the best approximation for each coefficient model.

V. Simulation Results

In [25] an initial approach on the identification of the Kadett 2400 aircraft model was performed. A MOOD strategy was also employed to achieve the aerodynamic stability and control derivatives. However, no wind estimation was made for compensating the sampled data. That work represents our starting point for this paper. Particularly, the models obtained in [25] are employed here to perform the simulations.

A simulation environment has been created as a validation tool in which the aircraft model can be subjected to different winds. Those winds are always known by the user, but the measured variables are GPS-like, in the sense that they refer to the Earth's surface and not to the air. In this way, if the estimated wind is similar to the one subjected to the model, it may be concluded that the technique successfully reached its objective. The spMODE algorithm is being employed. The decision space has been set as indicated in Eq. (11) but with the particularity of a maximum wind magnitude of 20 m/s. Different wind directions have been tested with similar results.

A. Constant Wind Simulations

In this first simulation, longitudinal and lateral experiments were conducted in which actuators were used independently to excite the system. A constant wind of 5 m/s with an elevation of $-20\,^\circ$ and a direction from North to South (*i.e.* $180\,^\circ$) was incorporated as the true wind. After the optimizer has completed the maximum number of generations it provides a set of solutions

in approximation to the Pareto set (Θ^*). Table 2 shows some values extracted from the set of solutions. First column in Table 2 gives the mean average of the set of solutions obtained for each experiment. It is a three-component vector that represents the wind vector $\mathbf{W} = (|\mathbf{W}|, \zeta, \xi)$ where $|\mathbf{W}|$ is expressed in m/s and ζ and ξ are expressed in rad. Values in the second column express the standard deviations of the whole set. The third and fourth columns give the absolute and relative errors of each component of the wind estimate.

Table 2: Simulation results for constant wind

Test type	**W mean** $\begin{bmatrix} \text{m/s} \\ \text{rad} \\ \text{rad} \end{bmatrix}$	**W standard deviation** $\begin{bmatrix} \text{m/s} \\ \text{rad} \\ \text{rad} \end{bmatrix}$	**W absolute error** $\begin{bmatrix} \text{m/s} \\ \text{rad} \\ \text{rad} \end{bmatrix}$	**W relative error** $\begin{bmatrix} \% \\ \% \\ \% \end{bmatrix}$
Elevators test	$\begin{bmatrix} 4.998988 \\ -0.353133 \\ 3.141773 \end{bmatrix}$	$\begin{bmatrix} 0.004948 \\ 0.000690 \\ 0.002964 \end{bmatrix}$	$\begin{bmatrix} 0.001012 \\ 0.004067 \\ 0.000181 \end{bmatrix}$	$\begin{bmatrix} 0.020242 \\ 1.165153 \\ 0.005754 \end{bmatrix}$
Motor test	$\begin{bmatrix} 4.947027 \\ -0.358709 \\ 3.140767 \end{bmatrix}$	$\begin{bmatrix} 0.031492 \\ 0.024524 \\ 0.012347 \end{bmatrix}$	$\begin{bmatrix} 0.052973 \\ 0.009643 \\ 0.000826 \end{bmatrix}$	$\begin{bmatrix} 1.059466 \\ 2.762445 \\ 0.026283 \end{bmatrix}$
Ailerons test	$\begin{bmatrix} 4.997899 \\ -0.349612 \\ 3.140767 \end{bmatrix}$	$\begin{bmatrix} 0.007045 \\ 0.002230 \\ 0.000613 \end{bmatrix}$	$\begin{bmatrix} 0.002101 \\ 0.000546 \\ 0.000826 \end{bmatrix}$	$\begin{bmatrix} 0.042013 \\ 0.156511 \\ 0.026277 \end{bmatrix}$
Rudder test	$\begin{bmatrix} 5.005375 \\ -0.351246 \\ 3.142247 \end{bmatrix}$	$\begin{bmatrix} 0.001417 \\ 0.000841 \\ 0.000307 \end{bmatrix}$	$\begin{bmatrix} 0.005375 \\ 0.002181 \\ 0.000654 \end{bmatrix}$	$\begin{bmatrix} 0.107498 \\ 0.624692 \\ 0.020826 \end{bmatrix}$

It can be seen that the estimation process converges to the actual wind with little error. It is interesting to see how, even for a constant wind and a known structure of the model, that estimated winds are not unique but a cloud of points very close to the real one. Two reasons may lead to this situation. First, the optimization problem has not been fully converged to the optimum value. Second, there are other (very similar) winds that explain discrepancies in the identification process as well as the real one. An observability issue can explain these discrepancies. This issue is fully

dependent on the type of experiment used for the estimation. As an example, in an elevator test in which the aircraft does not change yaw orientation, the optimizer does not observe how the wind azimuth affects the identification errors. As a result, there will be a whole set of winds with different azimuth angles explaining, as well as the real one, those identification errors in the aerodynamic coefficients. As will be later seen, this situation leads to a poor estimation of the wind in more realistic simulations in the case of longitudinal models.

B. Variable Wind Simulations

A second set of simulations were conducted in which the wind was modeled as a sinusoidal signal of $\left[5 + sin(\frac{2\pi}{10}t)\right]$ m/s, with a band limited white noise added to the azimuth and elevation angles. The nominal elevation ζ was again $-20\,^\circ$ while two different azimuth angles ξ were simulated: $180\,^\circ$ and $270\,^\circ$. In this case, a cloud of solutions around the nominal wind was expected, since there was no constant wind during the experiments.

Table 3 shows results for the north wind direction and Table 4 shows results for the east wind. Both tables include the same type of values shown in Table 2 but with different results. First, although the estimation errors were higher, the procedure is capable of estimating the simulated wind when lateral experiments were carried out. It is interesting to see how the error in the rudder test is higher than that observed in the ailerons test. This can also be explained by the variance in observability depending on the type of experiment. When a deflection in the ailerons is applied, the aircraft orientation relative to the wind vector covers a sufficiently wide range of values. On the contrary, when deflections are applied to the tail rudder, it is mostly the heading angle that changes, leading to a less observable experiment in terms of wind. Following the same reasoning, the first two rows of Table 3 and Table 4 represent the set of solutions proposed by the algorithm when the longitudinal tests are used in the procedure. The longitudinal experiments do not lead to a good estimation of the wind for any of the tested wind directions. Not only were the errors in the estimation higher, but the standard deviation of each set of solutions was also wider. To support this statement Fig. 7 has been included. As the graph shows, the real wind is among the cloud of solutions obtained by the MOEA: however, the cloud is so spread out that a reliable

wind estimation cannot be extracted. Again, this means that there is a whole set of winds with explaining, as well as the real one, those identification errors in the aerodynamic coefficients. By comparing Table 3 and Table 4 we can see that similar results were obtained for different wind azimuth angles. Hence, we can conclude that the longitudinal models suffer an observability issue in terms of wind estimation. This issue is also present in the rudder experiments but to a lesser degree. Therefore, the longitudinal experiments carried out here are inadequate for wind estimation purposes.

Table 3: Simulation results for variable wind

Test type	**W mean** $\begin{bmatrix} \text{m/s} \\ \text{rad} \\ \text{rad} \end{bmatrix}$	**W standard deviation** $\begin{bmatrix} \text{m/s} \\ \text{rad} \\ \text{rad} \end{bmatrix}$	**W absolute error** $\begin{bmatrix} \text{m/s} \\ \text{rad} \\ \text{rad} \end{bmatrix}$	**W relative error** $\begin{bmatrix} \% \\ \% \\ \% \end{bmatrix}$
Elevators test	$\begin{bmatrix} 7.966485 \\ -0.06888 \\ 3.406746 \end{bmatrix}$	$\begin{bmatrix} 2.96925 \\ 0.300134 \\ 1.105017 \end{bmatrix}$	$\begin{bmatrix} 2.966485 \\ 0.280186 \\ 0.265153 \end{bmatrix}$	$\begin{bmatrix} 59.329696 \\ 80.267362 \\ 8.440095 \end{bmatrix}$
Motor test	$\begin{bmatrix} 17.247653 \\ -0.554826 \\ 2.807634 \end{bmatrix}$	$\begin{bmatrix} 3.462794 \\ 0.663819 \\ 2.150964 \end{bmatrix}$	$\begin{bmatrix} 12.247653 \\ 0.20576 \\ 0.333959 \end{bmatrix}$	$\begin{bmatrix} 244.953066 \\ 58.945868 \\ 10.630239 \end{bmatrix}$
Ailerons test	$\begin{bmatrix} 5.268963 \\ -0.347613 \\ 3.038388 \end{bmatrix}$	$\begin{bmatrix} 0.011684 \\ 0.002634 \\ 0.022588 \end{bmatrix}$	$\begin{bmatrix} 0.268963 \\ 0.001453 \\ 0.103204 \end{bmatrix}$	$\begin{bmatrix} 5.379259 \\ 0.416195 \\ 3.285098 \end{bmatrix}$
Rudder test	$\begin{bmatrix} 5.521515 \\ -0.296587 \\ 2.720627 \end{bmatrix}$	$\begin{bmatrix} 0.033722 \\ 0.008135 \\ 0.021629 \end{bmatrix}$	$\begin{bmatrix} 0.521515 \\ 0.052479 \\ 0.420966 \end{bmatrix}$	$\begin{bmatrix} 10.430297 \\ 15.034222 \\ 13.399754 \end{bmatrix}$
Multiple actuators test	$\begin{bmatrix} 5.106339 \\ -0.393798 \\ 2.973994 \end{bmatrix}$	$\begin{bmatrix} 0.025308 \\ 0.00435 \\ 0.010241 \end{bmatrix}$	$\begin{bmatrix} 0.106339 \\ 0.044732 \\ 0.167599 \end{bmatrix}$	$\begin{bmatrix} 2.126776 \\ 12.814694 \\ 5.334845 \end{bmatrix}$

The implementation of experiments in which different actuators are excited simultaneously is proposed as a possible solution. Such a test could be used for wind estimation as well as for the

Table 4: Simulation results for variable wind

Test type	W mean $\begin{bmatrix} \text{m/s} \\ \text{rad} \\ \text{rad} \end{bmatrix}$	W standard deviation $\begin{bmatrix} \text{m/s} \\ \text{rad} \\ \text{rad} \end{bmatrix}$	W absolute error $\begin{bmatrix} \text{m/s} \\ \text{rad} \\ \text{rad} \end{bmatrix}$	W relative error $\begin{bmatrix} \% \\ \% \\ \% \end{bmatrix}$
Elevators test	$\begin{bmatrix} 4.344096 \\ -0.521659 \\ 4.314185 \end{bmatrix}$	$\begin{bmatrix} 1.408924 \\ 0.395895 \\ 1.187131 \end{bmatrix}$	$\begin{bmatrix} 0.655904 \\ 0.172594 \\ 0.398204 \end{bmatrix}$	$\begin{bmatrix} 13.118077 \\ 49.444434 \\ 8.450145 \end{bmatrix}$
Motor test	$\begin{bmatrix} 11.157674 \\ -0.07673 \\ 3.53739 \end{bmatrix}$	$\begin{bmatrix} 4.040244 \\ 0.350458 \\ 2.706765 \end{bmatrix}$	$\begin{bmatrix} 6.157674 \\ 0.272336 \\ 1.174999 \end{bmatrix}$	$\begin{bmatrix} 123.153488 \\ 78.018598 \\ 24.934243 \end{bmatrix}$
Ailerons test	$\begin{bmatrix} 5.129344 \\ -0.446838 \\ 4.461761 \end{bmatrix}$	$\begin{bmatrix} 0.030426 \\ 0.005952 \\ 0.002271 \end{bmatrix}$	$\begin{bmatrix} 0.129344 \\ 0.097773 \\ 0.250628 \end{bmatrix}$	$\begin{bmatrix} 2.586887 \\ 28.009761 \\ 5.318495 \end{bmatrix}$
Rudder test	$\begin{bmatrix} 4.74749 \\ -0.304223 \\ 3.917106 \end{bmatrix}$	$\begin{bmatrix} 0.83811 \\ 0.075543 \\ 0.110649 \end{bmatrix}$	$\begin{bmatrix} 0.25251 \\ 0.044843 \\ 0.795283 \end{bmatrix}$	$\begin{bmatrix} 5.050198 \\ 12.846522 \\ 16.87643 \end{bmatrix}$
Multiple actuators test	$\begin{bmatrix} 5.08521 \\ -0.275279 \\ 4.438785 \end{bmatrix}$	$\begin{bmatrix} 0.065749 \\ 0.007701 \\ 0.005862 \end{bmatrix}$	$\begin{bmatrix} 0.08521 \\ 0.073787 \\ 0.273604 \end{bmatrix}$	$\begin{bmatrix} 1.704192 \\ 21.138398 \\ 5.806064 \end{bmatrix}$

adjustment of all the stability and control derivatives. As a proof of concept, this type of test has been performed in simulation.

Figure 8 illustrates how the elevators, ailerons, and rudder are used during the experiment. Although this approach for applying input steps is not common, it is necessary due to time requirements. Time-skewed doublets could also be used here, but the authors want to highlight that the assumption of constant wind weakens as the duration of the experiments increase. In both cases, if the wind estimation is successful, it will be possible to use this information to correct the aerodynamic variables from the data and then accomplish an identification of both lateral and longitudinal models. The last row in Table 3 and Table 4 shows the wind estimation obtained for the same wind

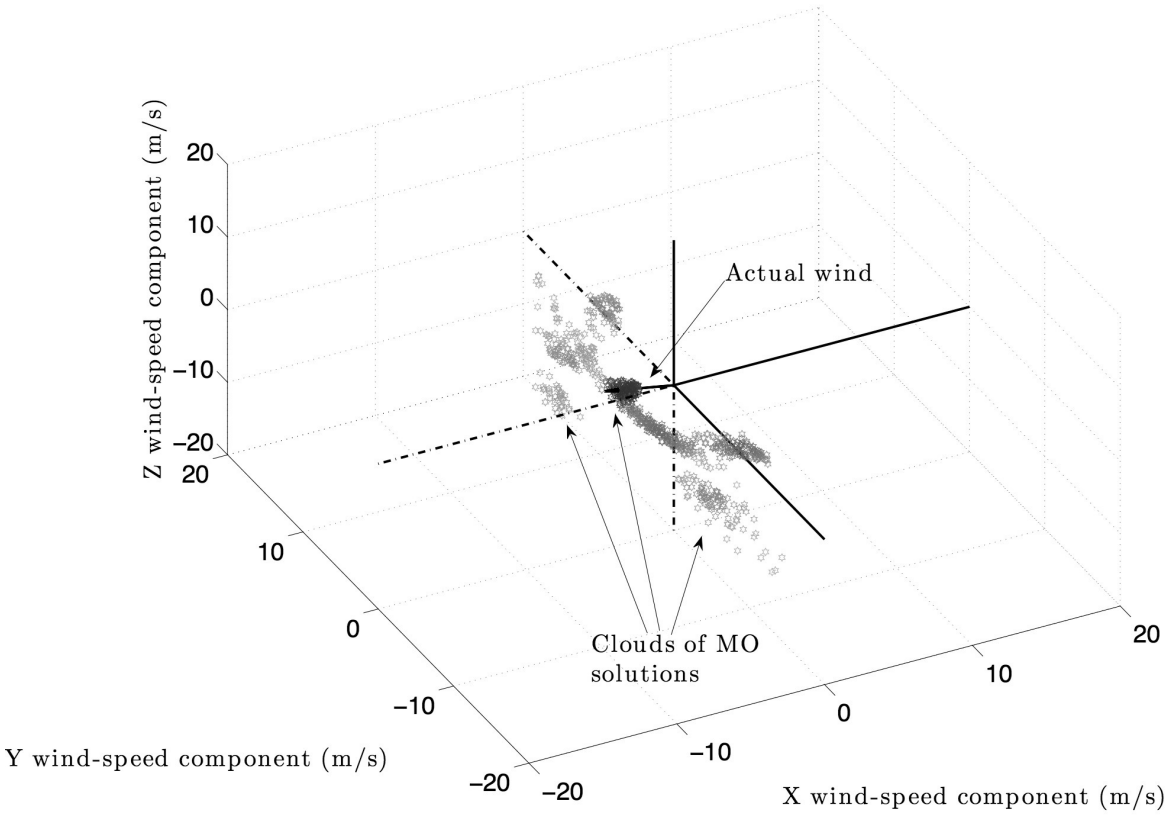

Fig. 7: Wind estimation results from simulation of elevators experiment with fluctuating wind

conditions as the previous cases. As can be observed, the wind estimation is accurately achieved this time.

Finally, Fig. 9 and Fig. 10 show the model identification results after the wind correction. When performing a simulation, models were already being used for each aerodynamic coefficient. Therefore, a distinction can be made between the actual value of the aerodynamic coefficient measured during simulation (continuous line) and the value obtained for each aerodynamic coefficient by taking the corrected regressors and using the simulation model to make a calculation (dashed line). The reader should note that these two values are only equal if the wind is correctly estimated and hence the regressors are perfectly corrected. The third variable depicted in Fig. 9 and Fig. 10

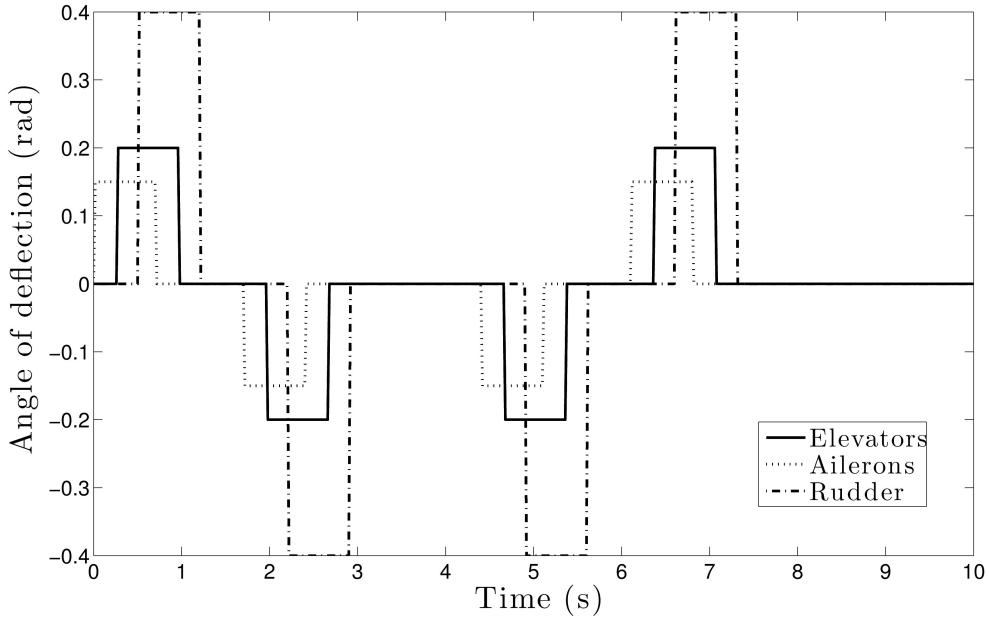

Fig. 8: Simulated experiment of multiple actuators

is the value of the coefficient that the newly identified model proposes with the corrected regressors (dotted line). It can be seen that all three are nearly superimposed, meaning a successful wind estimation and adjustment of the model parameters. Results show that both objectives can be accomplished simultaneously with this type of experiment.

VI. Experimental Results

A. Flight Tests

An aircraft which is maintaining constant heading and altitude, at a constant speed and with level wings (zero roll angle), is considered to be in steady flight. In the absence of disturbances, the pilot does not need to make any corrections to maintain this steady state.

To obtain data that can be employed in adjusting the aerodynamic parameters, step-input experiments have been performed. Thus, starting always from a steady-state flight such as the one described in the previous paragraph, each system input was manipulated separately and, after manipulation, the aircraft was left to evolve naturally, until the pilot deemed it appropriate to recover the aircraft. Each experiment was performed twice to obtain different data sets for identification

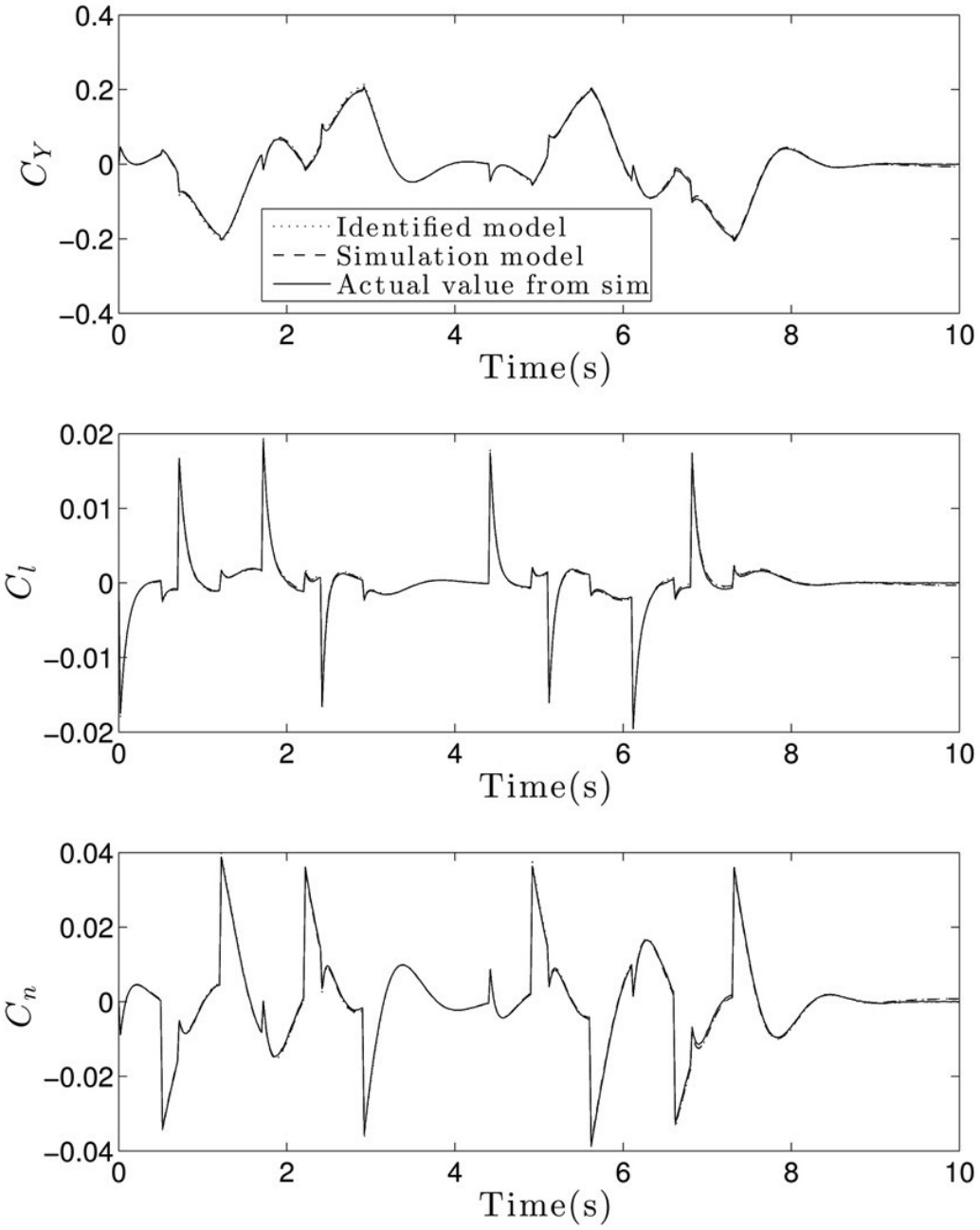

Fig. 9: Estimated lateral aerodynamic coefficients with simulation of multiple actuators

and validation. It should be noted that, in the absence of a sensor capable of measuring airspeed, all manoeuvres described below were carried out against the wind. This restriction was imposed on the pilot because of two reasons. First, to reduce variability between the flight tests. And second, due to the better wind estimation results obtained during the simulation phase.

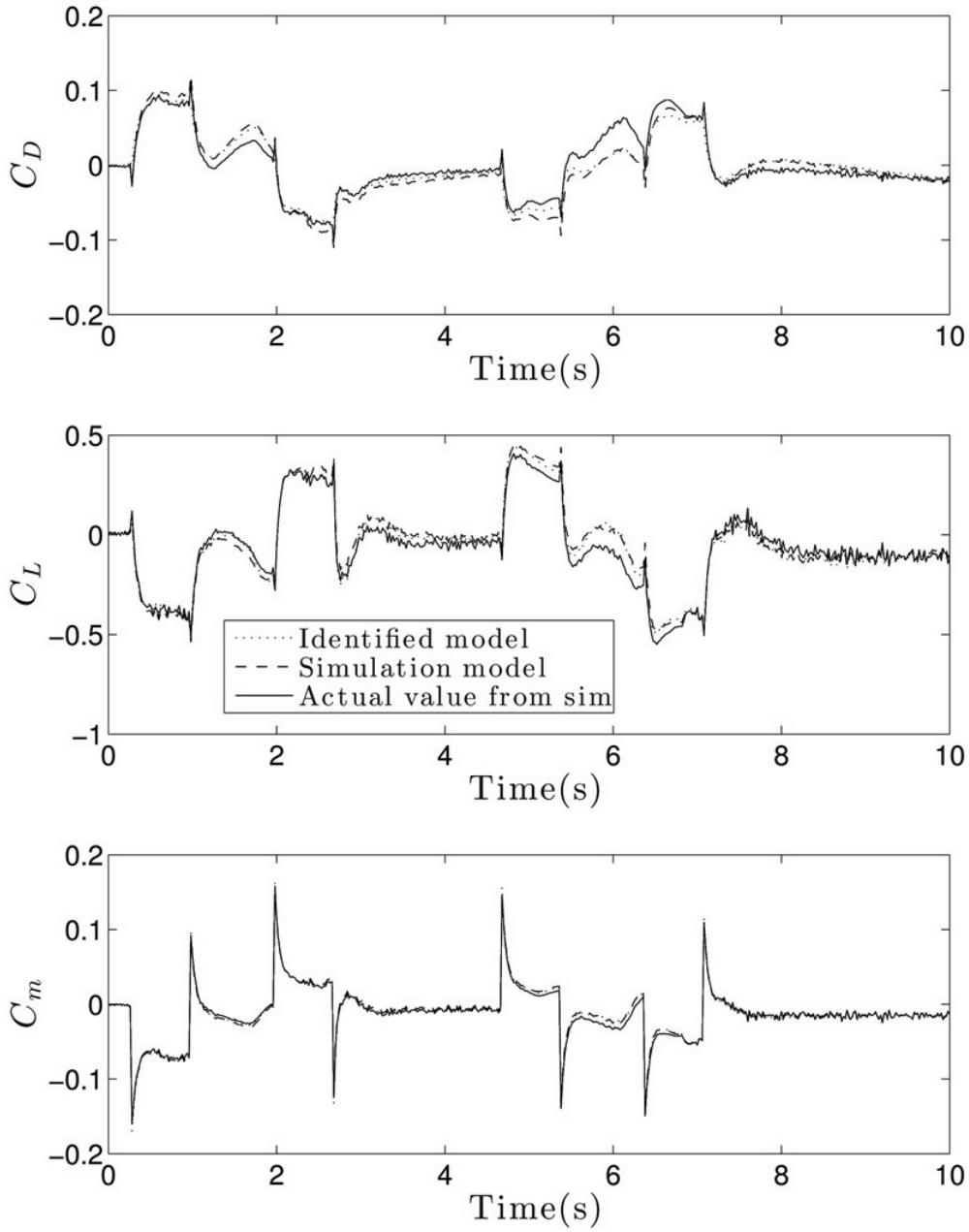

Fig. 10: Estimated longitudinal aerodynamic coefficients with simulation of multiple actuators

The flight plan provided to the pilot before beginning the experiments was:

1. Stable flight:
   (a) Adjust ailerons and rudder and level wings.
   (b) Set the motor load around 50%.

(c) Adjust elevators until the altitude remained constant without touching the control stick.

2. Elevators up and down to create a positive plus negative step sequence.

3. Repeat step 1.

4. Ailerons side to side in the appropriate frequency to avoid extreme rotations. First in one direction and then in the opposite direction.

5. Repeat step 1.

6. Tail rudder side to side. First in one direction and then in the opposite direction.

7. Repeat step 1.

8. Positive and negative steps in motor load. Sequence: 50%-100%-50%-0%-50%

9. Repeat the entire flight plan a second time.

Figure 11 and Fig. 12 show the evolution of the longitudinal and lateral variables during the elevator and aileron excitation tests, respectively. As shown, when a longitudinal input is activated, the remaining longitudinal variables are also activated, which finally produces variations in the symmetrical aerodynamic coefficients. This same behavior can be observed for the asymmetrical variables. All these variations can be collected and used to estimate the aerodynamic stability and control derivatives. As a final remark, Fig. 11 and Fig. 12 show the values $\hat{p} = \frac{b}{2V_0}p$, $\hat{q} = \frac{\bar{c}}{2V_0}p$, $\hat{r} = \frac{b}{2V_0}r$, $\hat{V} = \frac{1}{V_0}\Delta V_{air}$, and $\hat{\dot{\alpha}} = \frac{\bar{c}}{2V_0}\dot{\alpha}$. These are the values that multiply the stability and control derivatives in the aerodynamic coefficient models and, therefore, the regressors used in the identification procedure.

B. Wind Estimation Results

Separate step-input flight tests were performed to estimate the aerodynamic coefficient models. No experiment was carried out in which multiple control surfaces were employed at the same time. Thus, only lateral experiments were used in the wind estimation. For this reason, the information obtained from those tests is used to correct the longitudinal experiments as well.

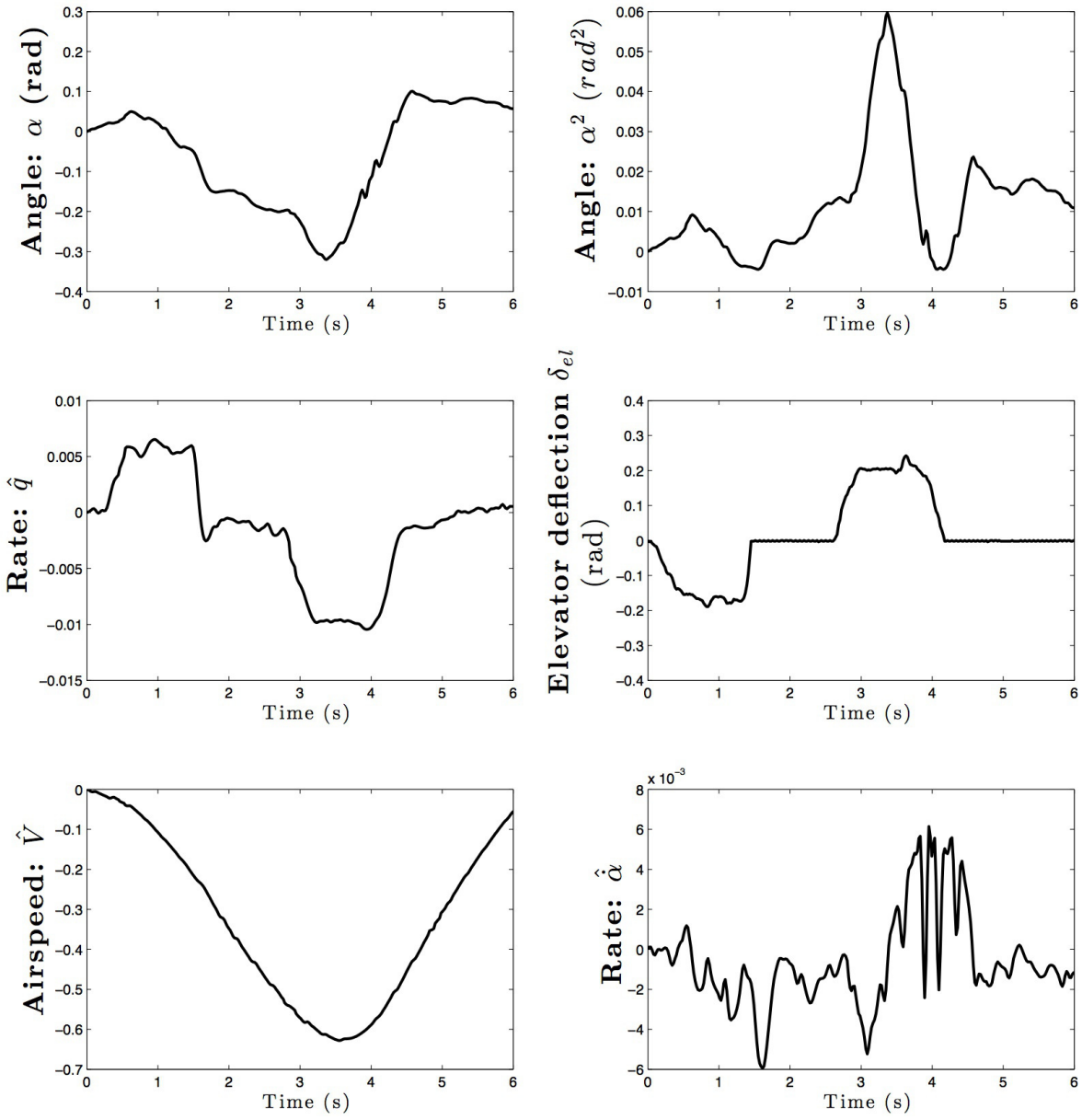

Fig. 11: Flight Test. Longitudinal variables evolution in an elevators test

Table 5 shows the set of solutions that the multi-objective optimizer converges to during the ailerons and rudder tests, respectively. Although wind direction and elevation vary slightly among sets, similar winds are obtained for every experiment. A population density criterion has been used in the final selection of one of the winds among all the solutions set. A sphere of radius $R = \max\{d_{ij}\}/20$ m/s around each solution has been placed for that purpose. The solution whose

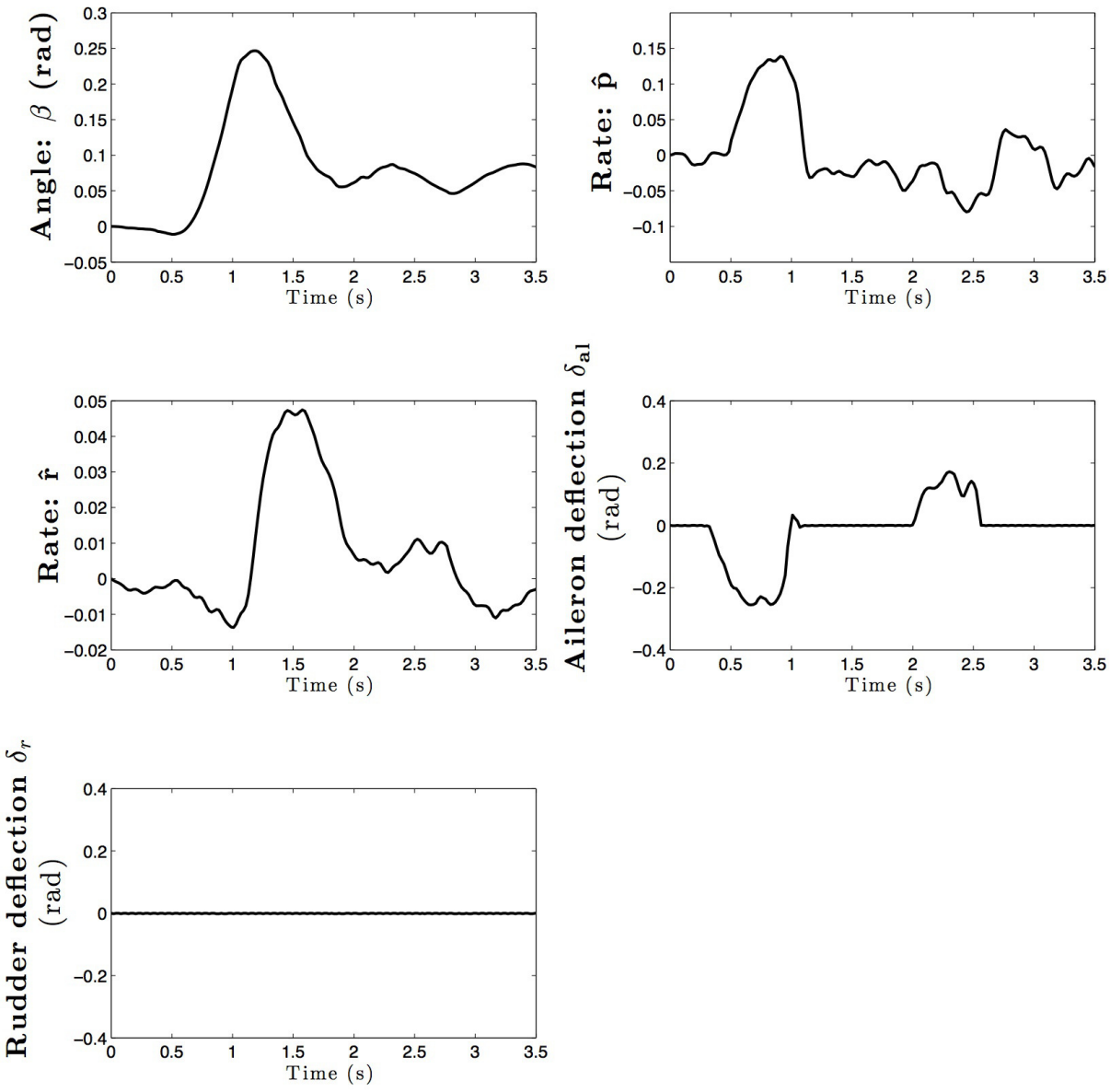

Fig. 12: Flight Test. Lateral variables evolution in an ailerons test

sphere contained the largest number of enclosed points was selected. That solution has been included in the third column of Table 5.

After selection, the MSE was computed in a cross validation analysis. Fewer quadratic errors were found for such validations than before correcting data. As an example, Fig. 13 shows the identification and validation mean squared errors found for the coefficient C_n with two different sets of data. Four groups of two bars are shown in Fig. 13. Given that there are two sets of data, each bar in a group represents the model identified using one of those two sets. In particular, the

Table 5: Wind estimation experimental results

Test type	W mean $\begin{bmatrix} \text{m/s} \\ \text{rad} \\ \text{rad} \end{bmatrix}$	W standard deviation $\begin{bmatrix} \text{m/s} \\ \text{rad} \\ \text{rad} \end{bmatrix}$	Chosen W $\begin{bmatrix} \text{m/s} \\ \text{rad} \\ \text{rad} \end{bmatrix}$
Ailerons test 1	$\begin{bmatrix} 8.490372 \\ -0.216576 \\ 5.437922 \end{bmatrix}$	$\begin{bmatrix} 0.906376 \\ 0.211093 \\ 0.027067 \end{bmatrix}$	$\begin{bmatrix} 8.283345 \\ -0.056781 \\ 5.449877 \end{bmatrix}$
Rudder test 1	$\begin{bmatrix} 9.811319 \\ -1.041670 \\ 5.352327 \end{bmatrix}$	$\begin{bmatrix} 1.789285 \\ 0.182896 \\ 0.105825 \end{bmatrix}$	$\begin{bmatrix} 10.133260 \\ -1.390814 \\ 5.992735 \end{bmatrix}$
Ailerons test 2	$\begin{bmatrix} 8.133613 \\ -1.071944 \\ 5.567295 \end{bmatrix}$	$\begin{bmatrix} 0.443366 \\ 0.200113 \\ 0.033953 \end{bmatrix}$	$\begin{bmatrix} 8.133613 \\ -1.071944 \\ 5.567295 \end{bmatrix}$
Rudder test 2	$\begin{bmatrix} 10.299536 \\ -0.869243 \\ 5.465950 \end{bmatrix}$	$\begin{bmatrix} 1.801400 \\ 0.168777 \\ 0.122687 \end{bmatrix}$	$\begin{bmatrix} 11.454439 \\ -1.249881 \\ 5.894774 \end{bmatrix}$

striped bar always represents the error for the model identified with Set 1, and the dotted bar the error for the model obtained with Set 2. Hence, the two groups on the right show the quadratic error found in the identification and the cross validation before the data was corrected with wind information. The two groups on the left give quadratic errors for identification and cross validation, once wind information was incorporated. It can be observed that quadratic errors have been reduced significantly (at least three times lower).

C. Identification Results

Once information about the wind acting during the flight tests is available, any airspeed-dependent variable may be corrected. With all the experimental data corrected, the process of finding the stability and control derivatives for each aerodynamic model began. Figure 14 and Fig. 15 show the Pareto fronts constituted by the possible models found by the algorithm for each aero-

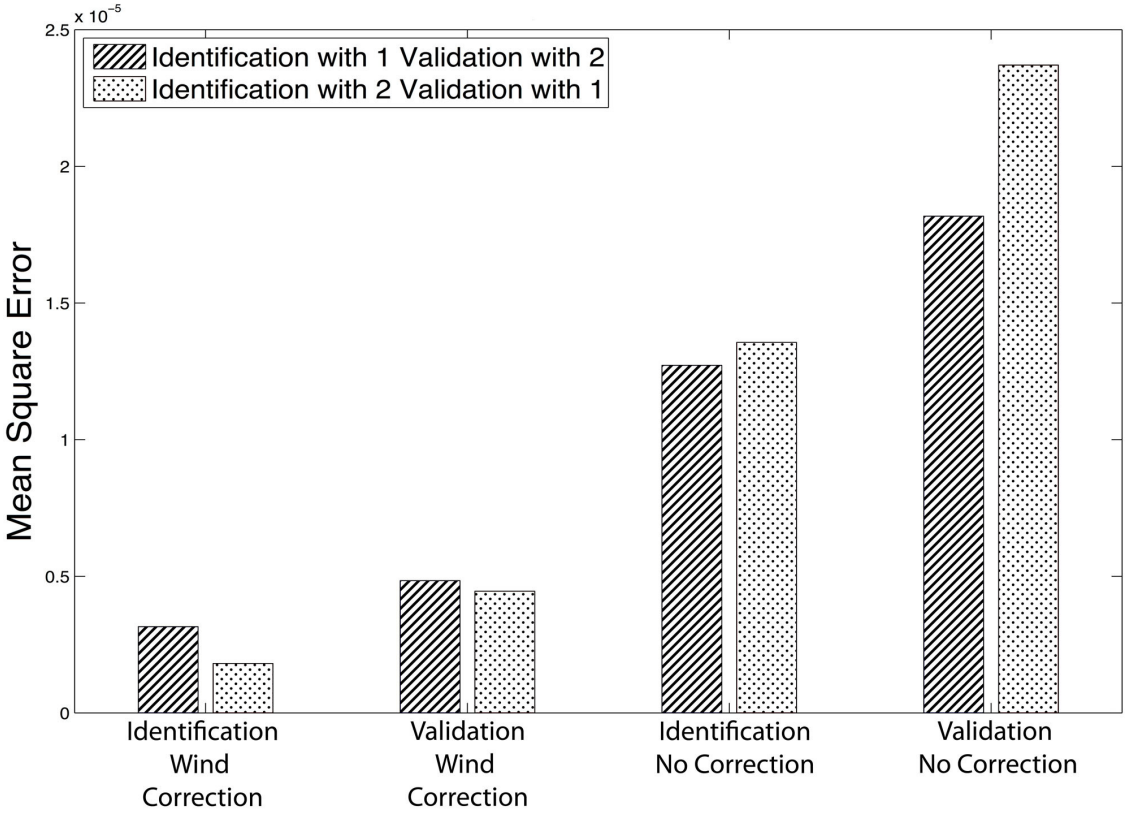

Fig. 13: C_n model mean squared errors: cross validation before and after wind correction

dynamic coefficient (hexagonal stars front). As can be seen, the better an experiment is fitted by a model, the more errors it obtains for a second test. This is why the person in charge of identifying the aircraft model cannot be satisfied after just one test, but should use the model with data from various experiments.

Moreover, testing experiments in a multi-objective optimization, instead of combining them in a mono-objective minimization, gives the main following advantages:

- Optimizing objectives separately results in solutions that could not be reachable if other optimization techniques are used (see Fig. 5).
- Using multi-objective optimization involves the selection of a solution among others, which gives the designer the power to define the importance of each experiment *a posteriori*, basing that definition on the requirements and the observed performance.

- The resultant Pareto front shows how good the different models are for each experiment. Thus, the designer may obtain an idea of how good the collected data is and so decide which are the requirements that should be satisfied in the final model.
- Flight conditions do not depend on the previous experiment.
- Duration of the experiments is the minimum required. This improves reliability on the wind estimation procedure.
- Metrics other than MSE can be used in the optimization.
- It is possible to add as many objectives as desired in the identification process. This means that comparing tests of the same type (*e.g.* two aileron tests and two rudder tests) is also possible, and this may prove to be a good practice for reducing variability.

For example, if the C_l coefficient is considered, it can be observed that the aileron tests produce a much better approximation than the rudder tests (see Fig. 14). This fact, which can be deduced from the mean squared error values, is also logical, since the ailerons introduce a moment about the roll axis. In this case, the designer should probably prefer models that fit better this type of experiment over models that do a better job with rudder tests.

With the intention of comparing solutions before and after wind correction, a second Pareto front was added to Fig. 14 and Fig. 15(triangles front). This front is the result of evaluating the Pareto set of solutions found by the MO algorithm when non-corrected flight data is used in the identification. As an interesting observation, Fig. 14 and Fig.15 illustrate that each Pareto front obtained with non-corrected flight data (dots front) is dominated by the corresponding Pareto front obtained with corrected flight data (hexagonal stars front). This means that the MSE of every model becomes smaller after correcting the flight data with the estimated wind.

The MOP ends with a multi-criteria decision making (MCDM) stage. In this case, a solution among the Pareto set will give us the final model parameters for each aerodynamic coefficient. Decision making is commonly a difficult task when many objectives and decision variables are involved. It is widely accepted that visualization tools are valuable and provide a meaningful method to analyze the Pareto front and take decisions [55]. Possibly the most common choices for Pareto

front visualization and analysis are: scatter diagrams, parallel coordinates [56], and level diagrams [57, 58]. In this work a level diagrams tool has been used to analyze Pareto fronts and Pareto sets and to decide a particular model for each coefficient. The final decision was made by taking into account the distance to the ideal solution, generated from the minimum values for each objective in the calculated Pareto front. This distance is a widely used metric in MCDM because it correctly represents the existing trade off among objectives. The squares on Fig. 14 are the selected models for each of the lateral aerodynamic coefficients. Those models represent a compromise between a situation in which the ailerons deflection is modified and a situation in which that modification is suffered by the tail rudder. This fact can be checked in Fig. 16. The graph shows the approximation given by the chosen model with validation data. Two more models from the Pareto set (circles on Fig. 14) have also been included in Fig. 16 (edge model 1 and edge model 2). Those two models have been named edge models here, and represent the best approximation in terms of MSE for the ailerons and rudder experiments separately (see [24]). The chosen MO solution (dotted curve) represents a good intermediate approximation in both situations. Finally, Table 6 presents validation results of every identified aerodynamic coefficient. Longitudinal coefficients have been subjected to validation data obtained in longitudinal experiments and, equally, lateral coefficients have been evaluated with validation sets obtained in lateral experiments. MSE presents similar values in identification and validation and so the identification may be taken as a success.

Table 6: Validation MSE

Aerodynamic coefficient	**Elevators experiment**	**Motor experiment**	**Ailerons experiment**	**Rudder experiment**
$\mathbf{C_D}$	0.000507759	0.000663917	-	-
$\mathbf{C_L}$	0.0058858	0.00145734	-	-
$\mathbf{C_Y}$	-	-	0.00166596	0.00122309
$\mathbf{C_l}$	-	-	$1.65789e-05$	$3.40064e-06$
$\mathbf{C_m}$	0.000326971	0.000167846	-	-
$\mathbf{C_n}$	-	-	$3.21581e-05$	$2.70232e-05$

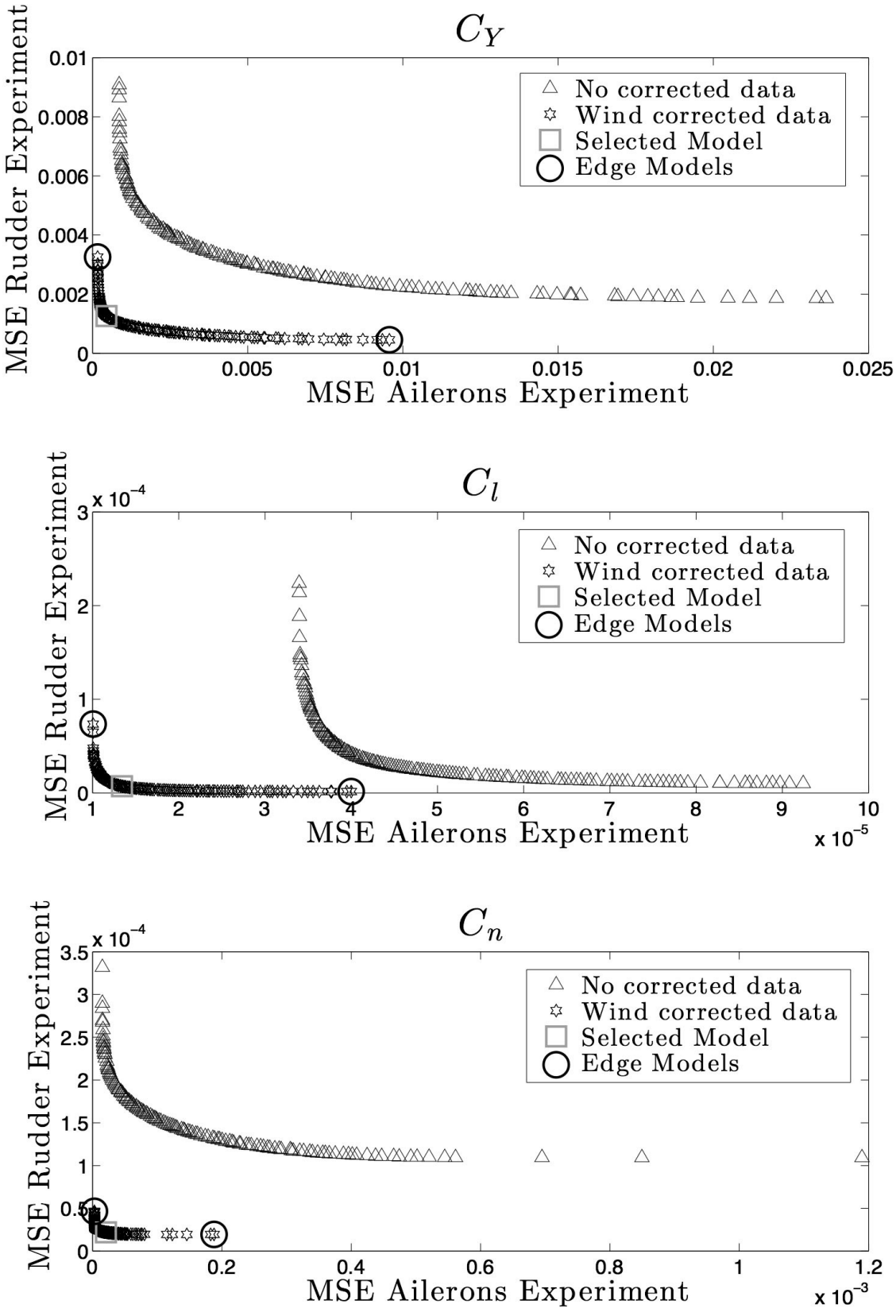

Fig. 14: MO Model Identification: control and stability derivatives for Lateral Aerodynamic Models

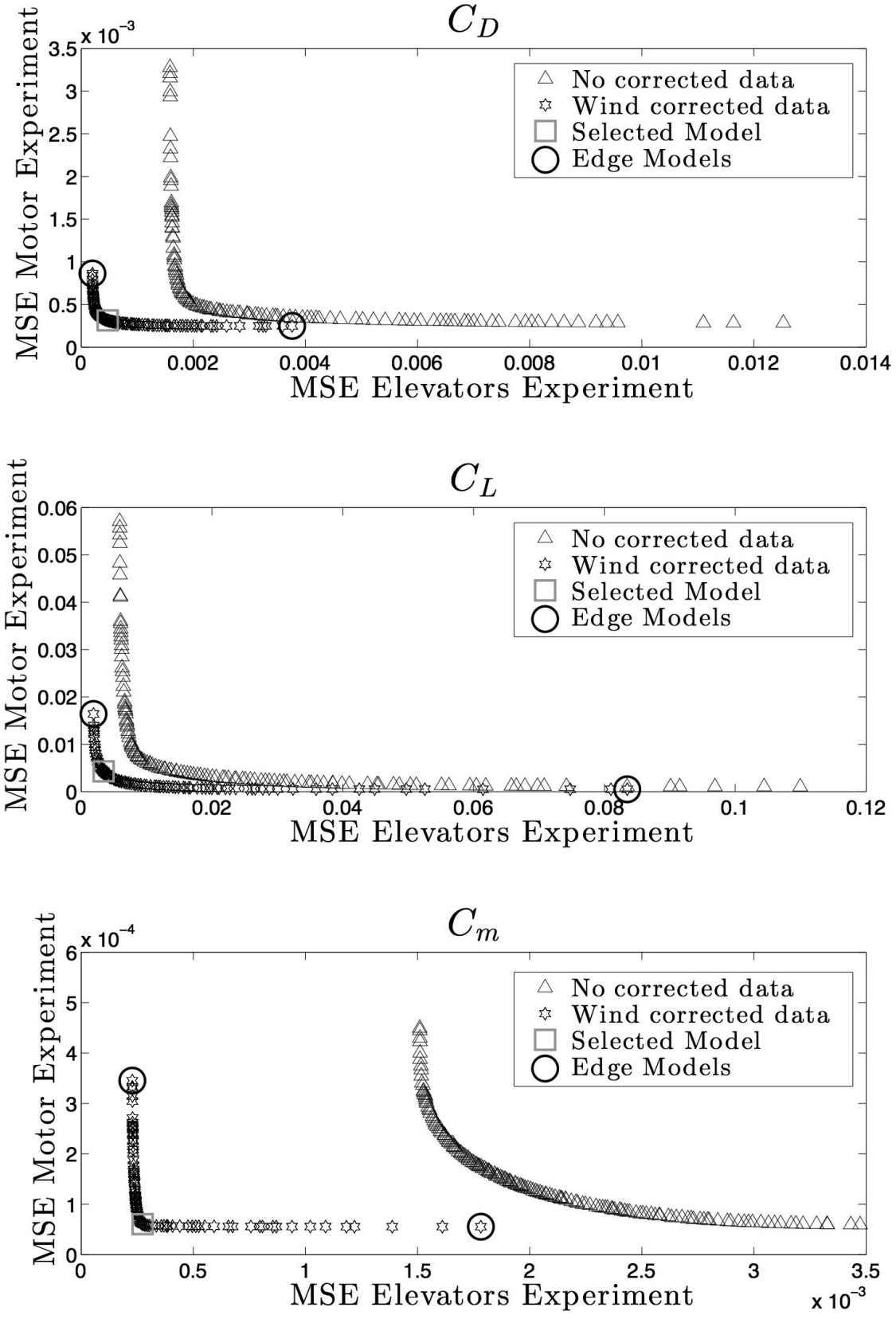

Fig. 15: MO Model Identification: control and stability derivatives for Longitudinal Aerodynamic Models

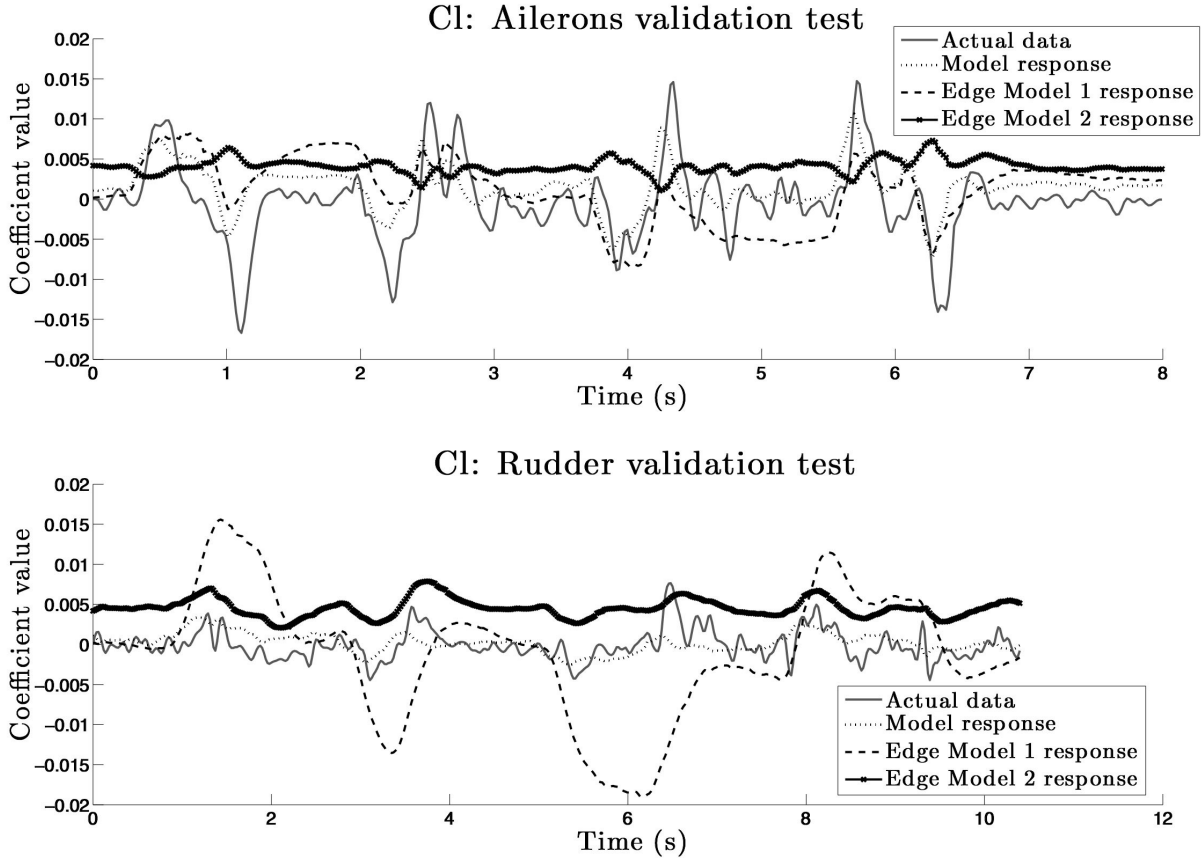

Fig. 16: C_l coefficient validation results

VII. Conclusions

A two-step identification technique for aerodynamic models of micro-air vehicles (MAV) in the absence of air-data sensors is presented. In the first step, a multi-objective optimization procedure is proposed to estimate wind during the flight experiments. A simulation environment that includes a MAV model that can be subjected to constant and variable winds was used to confirm the estimate process. Conditions in different flight tests in which one or more system inputs were excited were simulated, and after acquiring any necessary data from the simulations, the wind estimation technique was applied. Several conclusions can be extracted from these simulations. Firstly, under ideal conditions, wind estimation is successfully achieved in any experiment. Secondly, it can be concluded that only lateral experiments offer enough information to enable wind estimation under realistic conditions. Aircraft orientation relative to the wind azimuth does not vary during lon-

gitudinal experiments. Therefore, wind observability is significantly reduced. The same reason is reflected in the improved performance detected during the aileron experiments when compared with rudder experiments. Observability is improved when a wider range of orientation values are covered. For this reason, mixed experiments, *i.e.*, experiments that excite longitudinal and lateral variables simultaneously, achieved better results for wind estimation. As shown in section V B, this type of experiments can theoretically be used to estimate the wind and identify any of the aerodynamic coefficient models. But this fact has only been checked on simulation.

The same wind estimation procedure was applied to real flight data for lateral experiments. The obtained results infer that the wind was estimated and that the information obtained can be used to correct airspeed dependent measurements. As a final remark, the authors want to highlight that the estimation technique presented in this work is not intended to replace air-data sensors (whenever available). However, in those cases when no information at all can be used, a rough estimation of wind speed can significantly improve model quality. In addition, a similar multi-objective optimization approach might also be employed when partial airspeed information is available. That information could be incorporated in the optimization problem in order to improve airspeed measurements.

In the second step of the methodology, multi-objective optimization is again proposed to take advantage of the available flight data. The presented approach enables diverse experiments to be utilized, so that adjusting model parameters becomes, in reality, a multi-objective problem. This approach enabled us to obtain a compromise model that suited some flight situations without losing much performance in others. Furthermore, the visualization of the model fitness for several trials provides an idea of the quality of the obtained data and of the selected model structure. Although mean squared error has been used here, using a heuristic optimizer also enables the use of other performance indicators. For example, the mean absolute error is normally more meaningful to engineers because it has the same magnitude as the variable being modeled.

Acknowledgments

The authors would like to thank the Spanish Ministry of Innovation and Science for providing funding through the grant BES-2012-056210, and projects TIN-2011-28082 and ENE-25900. We also want to acknowledge the Generalitat Valenciana for financing this work through the project PROMETEO/2012/028.

References

[1] Krüll, W., Tobera, R., Willms, I., Essen, H., and von Wahl, N., "Early Forest Fire Detection and Verification using Optical Smoke, Gas and Microwave Sensors," in "2012 International Symposium on Safety Science and Technology," ELSEVIER, Vol. 45 of *Procedia Engineering*, 2012, pp. 584–594. Doi: 10.1016/j.proeng.2012.08.208.

[2] Xiang, H. and Tian, L., "Development of a low-cost agricultural remote sensing system based on an autonomous unmanned aerial vehicle (UAV)," *Biosystems engineering*, Vol. 108, No. 2, 2011, pp. 174–190.

[3] Prochazka, A., Kingsbury, N. G., Payner, P. J. W., and Uhlir, J., *Signal Analysis and Prediction*, Birkhä user Basel, Boston, MA, chap. System Identification, pp. 163–175, Applied and Numerical Harmonic Analysis, 1998.

[4] Iliff, K. W., "Parameter estimation for flight vehicles," *Journal of Guidance, Control, and Dynamics*, Vol. 12, No. 5, 1989, pp. 609–622,
doi:10.2514/3.20454.

[5] Hamel, P. G. and Jategaonkar, R. V., "Evolution of flight vehicle system identification," *Journal of Aircraft*, Vol. 33, No. 1, 1996, pp. 9–28,
doi:10.2514/3.46898.

[6] Wang, K. C. and Iliff, K. W., "Retrospective and Recent Examples of Aircraft Parameter Identification at NASA Dryden Flight Research Center," *Journal of Aircraft*, Vol. 41, No. 4, 2004, pp. 752–764,
doi:10.2514/1.332.

[7] Jategaonkar, R. V., Fischenberg, D., and Gruenhagen, W., "Aerodynamic Modeling and System Identification from Flight Data-Recent Applications at DLR," *Journal of Aircraft*, Vol. 41, No. 4, 2004, pp. 681–691,
doi:10.2514/1.3165.

[8] Morelli, E. A. and Klein, V., "Application of System Identification to Aircraft at NASA Langley Re-

search Center," *Journal of Aircraft*, Vol. 42, No. 1, 2005, pp. 12–25,
doi:10.2514/1.3648.

[9] Jategaonkar, R. V., *Flight vehicle system identification: a time domain methodology*, American Institute of Aeronautics and Astronautics, Vol. 216 of *Progress in astronautics and aeronautics*, chap. 10, pp. 335–375, 2006.

[10] Morelli, E. A., "Flight Test Maneuvers for Efficient Aerodynamic Modeling," *Journal of Aircraft*, Vol. 49, No. 6, 2012, pp. 1857–1867,
doi:10.2514/1.C031699.

[11] Dean, J., Morton, S., McDaniel, D., Clifton, J., and Bodkin, D., "Aircraft Stability and Control Characteristics Determined by System Identification of CFD Simulations," American Institute of Aeronautics and Astronautics, AIAA 2008-6378, 2008,
doi:10.2514/6.2008-6378.

[12] Rohlf, D., Schmidt, S., and Irving, J., "Stability and Control Analysis for an Unmanned Aircraft Configuration Using System-Identification Techniques," *Journal of Aircraft*, Vol. 49, No. 6, 2012, pp. 1597–1609,
doi:10.2514/1.C031392.

[13] Mueller, E. R., "Hardware-in-the-loop Simulation Design for Evaluation of Unmanned Aerial Vehicle Control Systems," in "Proceedings of AIAA Modeling and Simulation Technologies Conference," American Institute of Aeronautics and Astronautics, No. AIAA 2007-6569 in Guidance, Navigation, and Control and Co-located Conferences, 2007, pp. 530–543,
doi:10.2514/6.2007-6569.

[14] Cai, G., Chen, B. M., Lee, T. H., and Dong, M., "Design and implementation of a hardware-in-the-loop simulation system for small-scale UAV helicopters," *Mechatronics*, Vol. 19, No. 7, 2009, pp. 1057–1066.

[15] Wenbo, H. and Qiang, Z., "The Hardware-in-the-loop Simulation on the Control System of a Small Launch Vehicle," in "2012 International Workshop on Information and Electronics Engineering," ELSEVIER, Vol. 29 of *Procedia Engineering*, 2012, pp. 1867–1871. Doi:10.1016/j.proeng.2012.01.228.

[16] Watkins, S., Milbank, J., Loxton, B. J., and Melbourne, W. H., "Atmospheric Winds and Their Implications for Microair Vehicles," *AIAA Journal*, Vol. 44, No. 11, 2006, pp. 2591–2600,
doi:10.2514/1.22670.

[17] Mohamed, A., Massey, K., Watkins, S., and Clothier, R., "The attitude control of fixed-wing MAVS in turbulent environments," *Progress in Aerospace Sciences*, Vol. 66, No. 66, 2014, pp. 37–48,
doi:10.1016/j.paerosci.2013.12.003.

[18] Mohamed, A., Clothier, R., Watkins, S., Sabatini, R., and Abdulrahim, M., "Fixed-wing MAV attitude stability in atmospheric turbulence, part 1: Suitability of conventional sensors," *Progress in Aerospace Sciences*, Vol. 70, No. 70, 2014, pp. 69–82,
doi:10.1016/j.paerosci.2014.06.001.

[19] Rodriguez, A., Andersen, E., Bradley, J., and Taylor, C., "Wind Estimation Using an Optical Flow Sensor on a Miniature Air Vehicle," American Institute of Aeronautics and Astronautics, AIAA 2007-6614, 2007,
doi:10.2514/6.2007-6614.

[20] Langelaan, J. W., Alley, N., and Neidhoefer, J., "Wind Field Estimation for Small Unmanned Aerial Vehicles," *Journal of Guidance, Control, and Dynamics*, Vol. 34, No. 4, 2011, pp. 1016–1030,
doi:10.2514/1.52532.

[21] Cho, A., Kim, J., Lee, S., and Kee, C., "Wind estimation and airspeed calibration using a UAV with a single-antenna GPS receiver and pitot tube," *Aerospace and Electronic Systems, IEEE Transactions on*, Vol. 47, No. 1, 2011, pp. 109–117.

[22] Velasco, J., García-Nieto Rodríguez, S., Reynoso Meza, G., and Sanchis Saez, J., "Desarrollo y evaluación de una estación de control de tierra para vehículos aéreos no tripulados," in "Actas de las XXXIII Jornadas de Automática," Comité Español de Automática, 2012.

[23] Velasco, J., García-Nieto, S., Reynoso-Meza, G., and Sanchis, J., "Implementación de un sistema Hardware-In-the-Loop para la simulación en tiempo real de pilotos automáticos para UAVs," in "Actas de las XXXIV Jornadas de Automática," Comité Español de Automática, 2013.

[24] Velasco, J., *Identificación de modelos dinámicos y ajuste de controladores basado en algoritmos evolutivos multiobjetivo*, Master's thesis, Universidad Politécnica de Valencia, Spain, 2013.

[25] Velasco, J. and García-Nieto, S., "Unmanned Aerial Vehicles Model Identification Using Multi-Objective Optimization Techniques," in Edward, B., ed., "Proceedings of the 19th IFAC World Congress, 2014," International Federation of Automatic Control, Cape Town International Convention Centre, Cape Town, South Africa, Vol. 19 of *World Congress*, 2014, pp. 8837–8842,
doi:10.3182/20140824-6-ZA-1003.02023.

[26] Klein, V. and Morelli, E. A., *Aircraft system identification: theory and practice*, American Institute of Aeronautics and Astronautics, Inc., chap. 3, pp. 27–75, AIAA Education Series, 2006.

[27] Reynoso-Meza, G., *Design, coding and implementation of a multiobjective optimization algorithm based on Differential Evolution with spherical pruning: applications for system identification and controller tuning.*, Master's thesis, Universidad Politécnica de Valencia, Valencia, Spain, 2009.

[28] Miettinen, K., *Nonlinear multiobjective optimization*, Kluwer Academic Publishers, Boston, Vol. 12 of *International series in operations research & management science*, chap. Concepts, pp. 5–36, 1999.

[29] Sanchis, J., Martínez, M. A., Blasco, X., and Reynoso-Meza, G., "Modelling preferences in multi-objective engineering design," *Engineering Applications of Artificial Intelligence*, Vol. 23, No. 8, 2010, pp. 1255–1264,
doi:10.1016/j.engappai.2010.07.005.

[30] "Multi-Criteria Decision Making," in "Evolutionary Algorithms for Solving Multi-Objective Problems," Springer US, Genetic and Evolutionary Computation Series, pp. 515–545, 2007.

[31] Bonissone, P., Subbu, R., and Lizzi, J., "Multicriteria decision making (mcdm): a framework for research and applications," *Computational Intelligence Magazine, IEEE*, Vol. 4, No. 3, 2009, pp. 48–61,
doi:10.1109/MCI.2009.933093.

[32] Messac, A., Ismail-Yahaya, A., and Mattson, C. A., "The normalized normal constraint method for generating the Pareto frontier," *Structural and multidisciplinary optimization*, Vol. 25, No. 2, 2003, pp. 86–98.

[33] Sanchis, J., Martinez, M., Blasco, X., and Salcedo, J., "A new perspective on multiobjective optimization by enhanced normalized normal constraint method," *Structural and multidisciplinary optimization*, Vol. 36, No. 5, 2008, pp. 537–546.

[34] Das, I. and Dennis, J. E., "Normal-boundary intersection: A new method for generating the Pareto surface in nonlinear multicriteria optimization problems," *SIAM Journal on Optimization*, Vol. 8, No. 3, 1998, pp. 631–657.

[35] Messac, A. and Mattson, C. A., "Generating well-distributed sets of Pareto points for engineering design using physical programming," *Optimization and Engineering*, Vol. 3, No. 4, 2002, pp. 431–450.

[36] Zhou, A., Qu, B.-Y., Li, H., Zhao, S.-Z., Suganthan, P. N., and Zhang, Q., "Multiobjective evolutionary algorithms: A survey of the state of the art," *Swarm and Evolutionary Computation*, Vol. 1, No. 1, 2011, pp. 32–49.

[37] Coello, C. A. C., "Evolutionary multi-objective optimization: a historical view of the field," *Computational Intelligence Magazine, IEEE*, Vol. 1, No. 1, 2006, pp. 28–36.

[38] Srinivas, M. and Patnaik, L. M., "Genetic algorithms: A survey," *Computer*, Vol. 27, No. 6, 1994, pp. 17–26.

[39] Konak, A., Coit, D. W., and Smith, A. E., "Multi-objective optimization using genetic algorithms: A tutorial," *Reliability Engineering & System Safety*, Vol. 91, No. 9, 2006, pp. 992–1007.

[40] Kennedy, J. and Eberhart, R. C., "Particle swarm optimization," in "Proceedings of the 1995 IEEE

international conference on neural networks," IEEE Service Center, Piscataway, NJ., 1995, pp. 1942–1948.

[41] Coello, C. A. C., "An introduction to multi-objective particle swarm optimizers," in "Soft Computing in Industrial Applications," Springer, pp. 3–12, 2011.

[42] Storn, R. and Price, K., "Differential evolution: a simple and efficient heuristic for global optimization over continuous spaces," *Journal of global optimization*, Vol. 11, No. 4, 1997, pp. 341–359.

[43] Mezura-Montes, E., Reyes-Sierra, M., and Coello, C. A. C., "Multi-objective optimization using differential evolution: a survey of the state-of-the-art," in "Advances in differential evolution," Springer, pp. 173–196, 2008.

[44] Das, S. and Suganthan, P. N., "Differential evolution: a survey of the state-of-the-art," *Evolutionary Computation, IEEE Transactions on*, Vol. 15, No. 1, 2011, pp. 4–31.

[45] Karaboga, D., Gorkemli, B., Ozturk, C., and Karaboga, N., "A comprehensive survey: artificial bee colony (ABC) algorithm and applications," *Artificial Intelligence Review*, Vol. 42, No. 1, 2014, pp. 21–57.

[46] Dorigo, M. and Stützle, T., "Ant colony optimization: overview and recent advances," in "Handbook of metaheuristics," Springer, pp. 227–263, 2010.

[47] Reynoso-Meza, G., *Controller Tuning by Means of Evolutionary Multiobjective Optimization: a Holistic Multiobjective Optimization Design Procedure.*, Ph.D. thesis, Universidad Politecnica de Valencia, Valencia, Spain, 2014.

[48] Reynoso-Meza, G., Sanchis, J., Blasco, X., and Martínez, M., "Multi-objective Differential Evolution Algorithm with Spherical Pruning," *Matlab Central* [online database], URL: http://www.mathworks.ch/matlabcentral/fileexchange/47035-multi-objective-differential-evolution-algorithm-with-spherical-pruning-based-on-preferences [cited 15 June 2015].

[49] Reynoso-Meza, G., Sanchis, J., Blasco, X., and Martínez, M., "Design of Continuous Controllers Using a Multiobjective Differential Evolution Algorithm with Spherical Pruning," in Chio, C. and Cagnoni, S., eds., "Applications of Evolutionary Computation," Springer Berlin Heidelberg, Vol. 6024 of *Lecture Notes in Computer Science*, pp. 532–541, 2010.

[50] Cook, R. D. and Weisberg, S., *Residuals and influence in regression*, Chapman and Hall, New York, chap. Diagnostic methods using residuals, p. 18, Monographs on statistics and applied probability, 1982.

[51] Klein, V. and Morelli, E. A., *Aircraft system identification: theory and practice*, American Institute of Aeronautics and Astronautics, Inc., chap. 9, pp. 299–323, AIAA Education Series, 2006.

[52] Rodriguez-Vazquez, K. and Fleming, P. J., "Multi-objective genetic programming for nonlinear system

identification," *Electronics Letters*, Vol. 34, No. 9, 1998, pp. 930–931.

[53] Shih-Lian Cheng and Hwang, C., "Optimal approximation of linear systems by a differential evolution algorithm," *Systems, Man and Cybernetics, Part A: Systems and Humans, IEEE Transactions on*, Vol. 31, No. 6, 2001, pp. 698–707.

[54] Yousefi, H., Handroos, H., and Soleymani, A., "Application of Differential Evolution in system identification of a servo-hydraulic system with a flexible load," *Mechatronics*, Vol. 18, No. 9, 2008, pp. 513–528.

[55] Lotov, A. V. and Miettinen, K., "Visualizing the Pareto frontier," in Branke, J., Deb, K., Miettinen, K., and Slowinski, R., eds., "Multiobjective optimization," Springer, Berling Heidelberg, Vol. 5252 of *Lecture Notes in Computer Science*, pp. 213–243, 2008.

[56] Inselberg, A., "The plane with parallel coordinates," *The Visual Computer*, Vol. 1, No. 2, 1985, pp. 69–91.

[57] Blasco, X., Herrero, J., Sanchis, J., and Martínez, M., "A new graphical visualization of n-dimensional Pareto front for decision-making in multiobjective optimization," *Special Issue on Industrial Applications of Neural Networks 10th Engineering Applications of Neural Networks 2007*, Vol. 178, No. 20, 2008, pp. 3908–3924,
doi:10.1016/j.ins.2008.06.010.

[58] Reynoso-Meza, G., Blasco, X., Sanchis, J., and Herrero, J. M., "Comparison of design concepts in multi-criteria decision-making using level diagrams," *Information Sciences*, Vol. 221, No. 221, 2013, pp. 124–141. Doi:10.1016/j.ins.2012.09.049.